

Supporting Information

Atomically Accurate Site-Specific Ligand Tailoring of Highly Acid- and Alkali-Resistant Ti(IV)-based Metallamacrocycle for Enhanced CO₂ Photoreduction

Yi-Qi Tian,^{a‡} Lin-Fang Dai,^{a‡} Wen-Lei Mu,^a Wei-Dong Yu,^b Jun Yan,^{a*} Chao Liu^{a*}

^aHunan Provincial Key Laboratory of Chemical Power Sources, College of Chemistry and Chemical Engineering, Central South University, Changsha 410083, Hunan, P. R. China.

Correspondence and requests for materials should be addressed to C.L.

^bChina College of Science, Hunan University of Technology and Business, Changsha 410000, P. R. China.

Abstract: Skillfully engineering surface ligands at specific sites within robust clusters presents both a formidable challenge and a captivating opportunity. Herein we unveil an unprecedented titanium-oxo cluster: a calix[8]arene-stabilized metallamacrocycle (Ti₁₆L₄), uniquely crafted through the fusion of four "core-shell" {Ti₄@(TBC[8])(L)} subunits with four oxalate moieties. Notably, this cluster showcases an exceptional level of chemical stability, retaining its crystalline integrity even when immersed in highly concentrated acid (1M HNO₃) and alkali (20M NaOH). The macrocycle's surface unveils four specific, customizable μ₂-bridging sites, primed to accommodate diverse carboxylate ligands. This adaptability is highlighted through deliberate modifications achieved by alternating crystal soaking in alkali and carboxylic acid solutions. Furthermore, Ti₁₆L₄ macrocycles autonomously self-assemble into one-dimensional nanotubes, which subsequently organize into three distinct solid phases, contingent upon the specific nature of the four μ₂-bridging ligands. Notably, the Ti₁₆L₄ exhibit a remarkable capacity for photocatalytic activity in selectively reducing CO₂ to CO. Exploiting the macrocycle's modifiable shell yields a significant boost in performance, achieving an exceptional maximum CO release rate of 4.047 ± 0.243 mmol g⁻¹ h⁻¹. This study serves as a striking testament to the latent potential of precision-guided surface ligand manipulation within robust clusters, while also underpinning a platform for producing microporous materials endowed with a myriad of surface functionalities.

Contents

1. Experimental section.....	1
2. Detailed Structure Information for Ti ₁₆ L ₄ compounds.	7
3. Powder X-ray diffraction.....	16
4. XPS Measurement	19
5. TG-Measurement.....	20
6. IR spectra.....	21
7. Energy Dispersive X-ray (EDX) Spectroscopic Analysis	22
8. CO ₂ adsorption.....	23
9. Dynamic Light Scattering Measurement	23
10. Wettability of Ti ₁₆ L ₄ rings.....	24
11. Photocatalysis	24

1. Experimental section

Materials and Characterization. All reagents were purchased commercially and were not further purified when used. Powder X-ray diffraction (PXRD) analysis were performed on a Rigaku Mini Flex II diffractometer at a 2θ range of $5\text{--}50^\circ$ (5° min^{-1}) with $\text{CuK}\alpha$ radiation ($\lambda = 1.54056 \text{ \AA}$). The solid-state UV/Vis spectra data of the cluster samples were obtained on UV-4000 spectrophotometer. The diameters of cluster were measured by DLS using a Zetasizer Nano ZS90 (Malvern Instruments, UK). The measurements were conducted at a scattering angle of 90° at 25°C . The measurements were repeated thrice for each sample.

Synthesis for $[\text{H}_4\text{Ti}_{16}\text{O}_8(\text{TBC}[8])_4(\text{C}_2\text{O}_4)_4(\text{Ac})_4(\text{O}^i\text{Pr})_8] \cdot i\text{PrOH} \cdot 13\text{CH}_3\text{CN}$ (Ti₁₆L4-1**):** TBC[8] (28 mg, 0.021 mmol), Oxalic acid (27mg, 0.3 mmol), $\text{Eu}(\text{Ac})_3$ (33.4mg, 0.1mmol), and CH_3CN (5 mL) were added into a 25 mL Teflon lined stainless steel autoclave, and then added with $\text{Ti}(\text{O}^i\text{Pr})_4$ (200 μL , 0.65 mmol). The solution was sonicated for 5 min, then transferred to an oven at 120°C for 3 days. After it cool to room temperature, red stripe crystals of **Ti₁₆L4-1** were obtained. yield: 40% based on $\text{Ti}(\text{O}^i\text{Pr})_4$. The crystals are rinsed with CH_3CN and preserved under a sealed and dry environment. Elemental analysis calcd. (%) for $\text{C}_{423}\text{H}_{529}\text{N}_{14}\text{O}_{73}\text{Ti}_{16}$: C 65.60, H 6.88; found: C 64.63, H 6.57.

Synthesis for $[\text{H}_4\text{Ti}_{16}\text{O}_8(\text{TBC}[8])_4(\text{C}_2\text{O}_4)_4(\text{Ac})_2\text{Cl}_2(\text{O}^i\text{Pr})_8] \cdot 56\text{CH}_3\text{CN}$ (Ti₁₆L4-2**):** TBC[8](28 mg, 0.021 mmol), Oxalic acid (27mg, 0.3 mmol), EuCl_3 (25.8mg, 0.1mmol), $\text{Eu}(\text{Ac})_3$ (15mg, 0.045mmol) and CH_3CN (5 mL) were added into a 25 mL Teflon lined stainless steel autoclave, and then added with $\text{Ti}(\text{O}^i\text{Pr})_4$ (200 μL , 0.65 mmol). The solution was sonicated for 5 min, then transferred to an oven at 120°C for 3 days. After it cool to room temperature, red stripe crystals of **Ti₁₆L4-2** were obtained. yield: 32% based on $\text{Ti}(\text{O}^i\text{Pr})_4$. The crystals are rinsed with CH_3CN and preserved under a sealed and dry environment. Elemental analysis calcd. (%) for $\text{C}_{506}\text{H}_{648}\text{Cl}_2\text{N}_{59}\text{O}_{68}\text{Ti}_{16}$: C 64.09, H 6.89; found: C 63.29, H 6.51.

Synthesis for $[\text{H}_4\text{Ti}_{16}\text{O}_8(\text{TBC}[8])_4(\text{C}_2\text{O}_4)_4\text{Cl}_4(\text{O}^i\text{Pr})_8] \cdot 24\text{CH}_3\text{CN}$ (Ti₁₆L4-3**) :** TBC[8] (28 mg, 0.021 mmol), Oxalic acid (27mg, 0.3 mmol), EuCl_3 (25.8mg, 0.1mmol) and CH_3CN (5 mL) were added into a 25 mL Teflon lined stainless steel autoclave, and

then added with $\text{Ti}(\text{O}^i\text{Pr})_4$ (200 μL , 0.65 mmol). The solution was sonicated for 5 min, then transferred to an oven at 120 °C for 3 days. After it cool to room temperature, red stripe crystals of **Ti₁₆L₄-3** were obtained. yield: 12% based on $\text{Ti}(\text{O}^i\text{Pr})_4$. The crystals are rinsed with CH_3CN and preserved under a sealed and dry environment. Elemental analysis calcd. (%) for $\text{C}_{432}\text{H}_{536}\text{Cl}_4\text{N}_{24}\text{O}_{64}\text{Ti}_{16}$: C 64.88, H 6.76; found: C 64.13, H 6.24.

Synthesis for $[\text{Ti}_{16}\text{O}_8(\text{TBC}[8])_4(\text{C}_2\text{O}_4)_4(\text{Ac})_4(\text{O}^i\text{Pr})_4(\text{H}_2\text{O})_4]\cdot 23\text{H}_2\text{O}$ (**Ti₁₆L₄-1(a)**): 20 mg crystal of **Ti₁₆L₄-1** was immersed in 1M formic acid solution. After soaking for 24 hours, the red crystals of **Ti₁₆L₄-1(a)** were collected by filtration and washed with deionized water for three times.

Synthesis for $[\text{Ti}_{16}\text{O}_8(\text{TBC}[8])_4(\text{C}_2\text{O}_4)_4(\text{Fa})_4(\text{O}^i\text{Pr})_4(\text{H}_2\text{O})_4]\cdot 3\text{CH}_3\text{CN}\cdot 24\text{H}_2\text{O}$ (**Ti₁₆L₄-1/HFa(a)**): 20 mg crystal of **Ti₁₆L₄-1** was immersed in 5M formic acid solution. After soaking for 24 hours, the red crystals of **Ti₁₆L₄-1/HFa(a)** were collected by filtration and washed with deionized water for three times.

Synthesis for $[\text{Na}_8\text{Ti}_{16}\text{O}_8(\text{TBC}[8])_4(\text{C}_2\text{O}_4)_4(\text{OH})_{16}(\text{H}_2\text{O})_{12}(\text{CH}_3\text{CN})]\cdot 2\text{CH}_3\text{CN}\cdot 55\text{H}_2\text{O}$ (**Ti₁₆L₄-1/NaOH**): 20 mg crystal of **Ti₁₆L₄-1** was immersed in 5M NaOH. The color of the crystal gradually changes from red to yellow. After soaking for 30min, the yellow crystals of **Ti₁₆L₄-1/NaOH** were collected by filtration and washed with deionized water for three times.

Synthesis for $[\text{Na}_4\text{Ti}_{16}\text{O}_8(\text{TBC}[8])_4(\text{C}_2\text{O}_4)_4(\text{Fa})_4(\text{OH})_8(\text{H}_2\text{O})_4]\cdot 34\text{H}_2\text{O}$ (**Ti₁₆L₄-1/HFa(b)**): 20mg crystal of **Ti₁₆L₄-1/NaOH** was immersed in 1M formic acid solution. The color of the crystal gradually changes from yellow to red. After soaking for 30min, the yellow crystals of **Ti₁₆L₄-1/HFa(b)** were collected by filtration and washed with deionized water for three times.

Synthesis for $[\text{Ti}_{16}\text{O}_8(\text{TBC}[8])_4(\text{C}_2\text{O}_4)_4(\text{Cl}_a)_4(\text{O}^i\text{Pr})_4(\text{H}_2\text{O})_4]\cdot 38\text{H}_2\text{O}$ (**Ti₁₆L₄-1/HCl_a**): 20mg crystal of **Ti₁₆L₄-1** was immersed in 5M chloroacetic acid solution. After soaking for 24 hours, the red crystals of **Ti₁₆L₄-1/HCl_a** were collected by filtration and washed with deionized water for three times.

Synthesis for $[\text{Ti}_{16}\text{O}_8(\text{TBC}[8])_4(\text{C}_2\text{O}_4)_4(\text{Bra})_4(\text{O}^i\text{Pr})_4(\text{H}_2\text{O})_4]\cdot 38\text{H}_2\text{O}$ (**Ti₁₆L₄-1/HBra**): 20mg crystal of **Ti₁₆L₄-1** was immersed in 5M trifluoroacetic acid solution.

After soaking for 24 hours, the red crystals of **Ti₁₆L₄-1**/HBra were collected by filtration and washed with deionized water for three times.

Synthesis for $[\text{Na}_2\text{Ti}_{16}\text{O}_8(\text{TBC}[8])_4(\text{C}_2\text{O}_4)_4(\text{Ac})_{10}(\text{HAc})_6]\cdot 2\text{HAc}\cdot 49\text{H}_2\text{O}$ (**Ti₁₆L₄-1**/HAc): 20mg crystal of **Ti₁₆L₄-1**/NaOH was immersed in 1M acetic acid solution, and the crystal color gradually changes from red to yellow. After soaking for 30min, the red crystals of **Ti₁₆L₄-1**/HAc were collected by filtration and washed with deionized water for three times.

Synthesis for $[\text{Na}_4\text{Ti}_{16}\text{O}_8(\text{TBC}[8])_4(\text{C}_2\text{O}_4)_4(\text{Ama})_8(\text{H}_2\text{O})_{12}]$ (**Ti₁₆L₄-1**/HAma): 20mg crystal of **Ti₁₆L₄-1**/NaOH was immersed in 1M aminoacetic acid solution, and the crystal color gradually changed from yellow to red after 30 min. The red crystals of **Ti₁₆L₄-1**/HAma were collected by filtration and washed with deionized water for three times.

Synthesis for $[\text{Ti}_{16}\text{O}_8(\text{TBC}[8])_4(\text{C}_2\text{O}_4)_4(\text{Oa})_4(\text{OH})_4(\text{H}_2\text{O})_4]\cdot 49\text{H}_2\text{O}$ (**Ti₁₆L₄-1**/H₂Oa): 20mg crystal of **Ti₁₆L₄-1**/NaOH was immersed in 1M oxalic acid solution, and the crystal color gradually changed from yellow to red. After soaking for 30min, the red crystals of **Ti₁₆L₄-1**/H₂Oa were collected by filtration and washed with deionized water for three times.

Synthesis for $[\text{Ti}_{16}\text{O}_8(\text{TBC}[8])_4(\text{C}_2\text{O}_4)_4(\text{Ga})_4(\text{OH})_4(\text{H}_2\text{O})_4]\cdot 2\text{CH}_3\text{CN}\cdot 45\text{H}_2\text{O}$ (**Ti₁₆L₄-1**/HGa): 20mg crystal of **Ti₁₆L₄-1**/NaOH was immersed in 1M glycolic acid solution, and the crystal color changed from yellow to red. After soaking for 30min, the red crystals of **Ti₁₆L₄-1**/HGa were collected by filtration and washed with deionized water for three times.

Synthesis for $[\text{Ti}_{16}\text{O}_8(\text{TBC}[8])_4(\text{C}_2\text{O}_4)_4(\text{Tfa})_4(\text{O}^i\text{Pr})_4(\text{H}_2\text{O})_4]\cdot 38\text{H}_2\text{O}$ (**Ti₁₆L₄-12**/HTfa): 20mg crystal of **Ti₁₆L₄-2** was immersed in 5M trifluoroacetic acid solution. After soaking for 24 hours, the red crystals of **Ti₁₆L₄-1**/HTfa were collected by filtration and washed with deionized water for three times.

Synthesis for $[\text{Ti}_{16}\text{O}_8(\text{TBC}[8])_4(\text{C}_2\text{O}_4)_4(\text{OH})_8(\text{H}_2\text{O})_4]\cdot 4\text{H}_2\text{O}$ (**Ti₁₆L₄-1**/H₃PO₄): 20mg crystal of **Ti₁₆L₄-1**/NaOH was immersed in 1M phosphoric acid solution, and the crystal color changed from yellow to red. After soaking for 30min, the red crystals of

Ti₁₆L₄-1/OH⁻ were collected by filtration and washed with deionized water for three times.

X-ray Crystallographic Analyses. Crystallographic data of all the crystals were collected on Bruker D8 Venture diffractometer with liquid metal Ga-K α radiation ($\lambda = 1.3405 \text{ \AA}$) at about 100 K. Absorption correction was applied using SADABS.¹ The structures were solved with the dual-direct methods using ShelxT and refined with the full-matrix least-squares technique based on F^2 using the SHELXL-2014.^{2, 3} Non-hydrogen atoms were refined anisotropically. Due to the rotation disorder of tert-butyl groups, in all cases the ISOR, DELU and SIMU constraints were necessary to achieve convergence. Hydrogen atoms were added theoretically, riding on the concerned atoms and refined with fixed thermal factors. Hydrogen atoms bonded to oxygen (water and hydroxyl ions) were not located from difference maps or included in the refinement. Besides, some water molecule is severely disordered and the related hydrogen atoms were not included. For all the clusters, the highly disordered solvent molecules in the crystal structures were removed with the SQUEEZE program in PLATON. All absorption corrections were performed using the multiscan program. The obtained crystallographic data for these cluster are summarized in Table S1 to Table S2.

Reference:

1. Sheldrick, G. M. SADABS: Program for Area Detector Adsorption Correction; University of Göttingen: Göttingen, Germany, 1996.
2. Sheldrick, G. M. SHELXL-2014/7: A Program for Structure Refinement; University of Göttingen: Göttingen, Germany, 2014.
3. Dolomanov, O. V.; Bourhis, L. J.; Gildea, R. J. J.; Howard, A. K.; Puschmann, H. OLEX²: a complete structure solution, refinement and analysis program. *J. Appl. Crystallogr.* 2009, 42, 339–341.

Preparation of active samples for gas adsorption Crystals were soaked in ethanol and heated at 80 °C for three days. During this time, the ethanol solution should be exchanged several times a day. Subsequently, the sample was degassed under a dynamic vacuum at 100 °C for 6 h to activate the sample. The gas adsorption isotherms of active samples were obtained on a Micromeritics ASAP 2020 volumetric adsorption instrument.

Photoelectrochemical measurements were performed on a CHI 660e electrochemical workstation in a standard three-electrode electrochemical cell with a working electrode,

a platinum plate as the counter electrode, and a saturated calomel electrode as the reference electrode. These three electrodes were immersed in the 0.2M Na₂SO₄ aqueous solution (pH = 6.6). A 300 W high-pressure xenon lamp with UV cut-off filter was used as a full-wavelength light source, located 20 cm away from the working electrode. The colloidal dispersion was obtained by ultrasonic treatment of 5 mg ground crystal sample in 1 ml ethanol for 30 min, and then the dispersion was dropped onto FTO glass (0.75 cm² area). After evaporation under an ambient atmosphere for 2 h, the coating film was obtained and used as the working electrode. Mott-Schottky plots were recorded at frequencies of 600, 800, and 1000 Hz, respectively.

Contact Angle Measurements. Contact angles were measured on powder samples using a contact angle meter with a rotatable substrate holder. To perform contact angle measurements, 20 mg of powder samples of the clusters were deposited on a glass substrate bed. Then, powders were pressed to make a flat surface by the glass slide. A 10 μ L water droplet was released slowly on the flat surface of the powder samples. The droplet image was taken by a high-performance charge-coupled device (CCD) sensor. The contact angle of all powder samples was analyzed by five-point simulation analysis.

Photocatalytic experiments. The photocatalytic experiments were performed in a 100 mL optical reaction vessel with stirring at ambient temperature. A mixture of 3 mg photocatalyst, 10 mg [Ru(bpy)₃]Cl₂·6H₂O and 5 mL triethanolamine (TEOA) was put into optical reaction vessel, followed by the addition of 8 mL acetonitrile and 2 mL deionized water. After homogeneous mixing, the suspension was stirred and purged with carbon dioxide for 10 min to remove air. A 300 W Xe lamp equipped with a UV cut-off filter ($\lambda \geq 420$ nm) was utilized as the light source. For each evaluation of gaseous products, 400 μ L of the headspace was injected into the gas chromatography (Shimadzu GC2014, argon as a carrier gas) every hour.

In situ diffuse reflectance infrared Fourier transform spectroscopy (DRIFTS) measurements. In situ DRIFTS over **Ti₁₆L₄_1** was obtained by using a Bruker INVENIO S FT-IR spectrophotometer, equipped with an MCT detector cooled by liquid nitrogen and a commercial reaction chamber from Harrick Scientific. The sample

was degassed at 373 K in N₂ atmosphere for 30 min, and then the gas flow was switched to pure CO₂ through deionized water for adsorption at room temperature. The sample was irradiated by the Xe lamp through a quartz window. The gaseous mixture of CO₂ and H₂O vapor were steadily produced before the measurement. The background spectrum was collected after 10 min of adsorption in pure CO₂. After then, the IR spectra were collected in situ through the MCT detector. Each spectrum was recorded by averaging 64 scans at a 4 cm⁻¹ spectral resolution.

2. Detailed Structure Information for Ti₁₆L₄ Compounds.

Table S1: Crystallographic data of the three Ti₁₆L₄ compounds.

Compounds	Ti ₁₆ L ₄ _1	Ti ₁₆ L ₄ _2	Ti ₁₆ L ₄ _3
CCDC	2174429	2174430	2174431
Cryst. syst.	monoclinic	monoclinic	tetragonal
Space group	C2/c	C2/c	I422
Formula	C ₄₂₃ H ₅₂₉ N ₁₄ O ₇₃ Ti ₁₆	C ₃₉₆ H ₄₈₄ Cl ₂ N ₄ O ₆₈ Ti ₁₆	C ₄₃₂ H ₅₃₆ Cl ₄ N ₂₄ O ₆₄ Ti ₁₆
Fw	7743.97	7225.14	7997.02
<i>a</i> [Å]	39.1900(19)	53.303(2)	38.021(13)
<i>b</i> [Å]	32.5046(16)	19.9467(8)	38.021(13)
<i>c</i> [Å]	38.1646(18)	50.645(2)	19.702(4)
β [°]	115.461(2)	121.288(2)	90
<i>V</i> [Å ³]	43894(4)	46016(3)	28481(20)
<i>Z</i>	4	4	2
$\rho_{\text{calc}}/\text{cm}^3$	1.079	1.067	0.933
μ/mm^{-1}	1.921	1.818	1.618
<i>F</i> (000)	15216.0	15623.0	8456.0
Data/restraints/parameters	38766/325/2344	40607/275/2453	10299/535/648
Goof	1.105	1.031	1.009
R ₁ /wR ₂ (I > 2σ(I))	0.0997/0.2961	0.0950/0.2783	0.0622/0.1693
R ₁ /wR ₂ (all data)	0.1166/0.3132	0.1070/0.2930	0.0888/0.1865

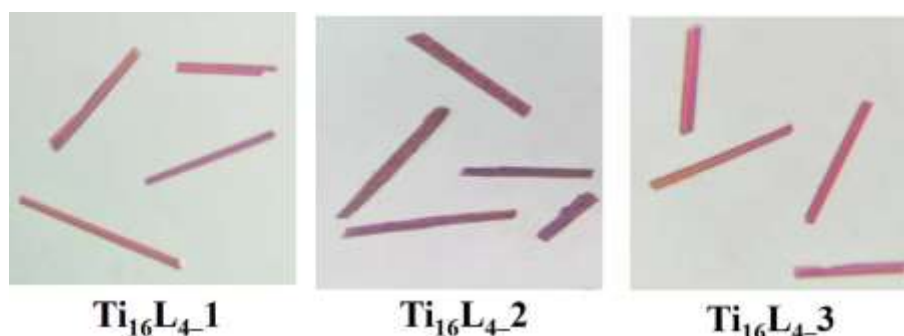


Figure S1. Pictures of fresh crystals of three Ti₁₆L₄ clusters separated from the solution.

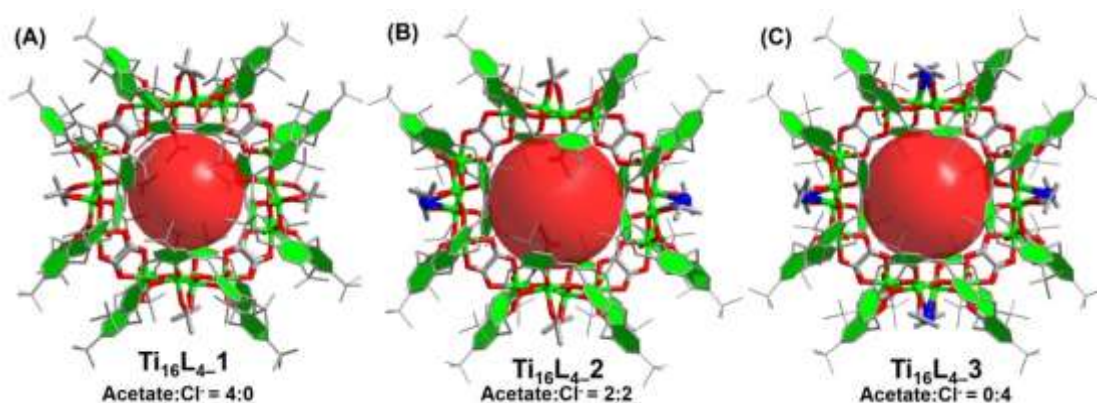


Figure S2. Crystal structures of the three Ti_{16}L_4 clusters.

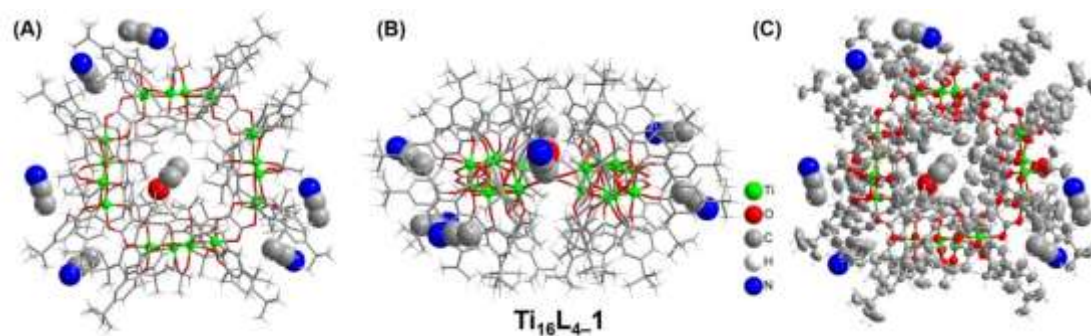


Figure S3. The molecular structure of $\text{Ti}_{16}\text{L}_4\mathbf{1}$. (a) and (a) The ball-and-stick view; (b) the ORTEP-style view.

$\text{Ti}_{16}\text{L}_4\mathbf{1}$ is isolated from the acetonitrile. The molecular formula of $\text{Ti}_{16}\text{L}_4\mathbf{1}$ was determined as $[\text{H}_4\text{Ti}_{16}\text{O}_8(\text{TBC}[8])_4(\text{C}_2\text{O}_4)_4(\text{Ac})_4(\text{O}^i\text{Pr})_8]^{-1}\text{PrOH}\cdot 13\text{CH}_3\text{CN}$. Some highly disordered solvent molecules in the crystal structures were removed with the SQUEEZE program in PLATON, and its possible formula was proposed based on the SQUEEZE and TGA results. SCXRD analysis showed the position of some guest molecules. An $^i\text{PrOH}$ guest is located inside the macrocycle. Outside the macrocycle, there are CH_3CN^- molecules located at the cup mouth of $\text{TBC}[8]$. Interestingly, in Ti_{16}L_4 , two $\text{TBC}[8]$ are adjacent to each other to form a smaller pocket in which a CH_3CN^- molecule is anchored through hydrogen bond interactions. The average $\text{C}\cdots\text{H}\cdots\text{N}$ lengths is 2.994 Å.

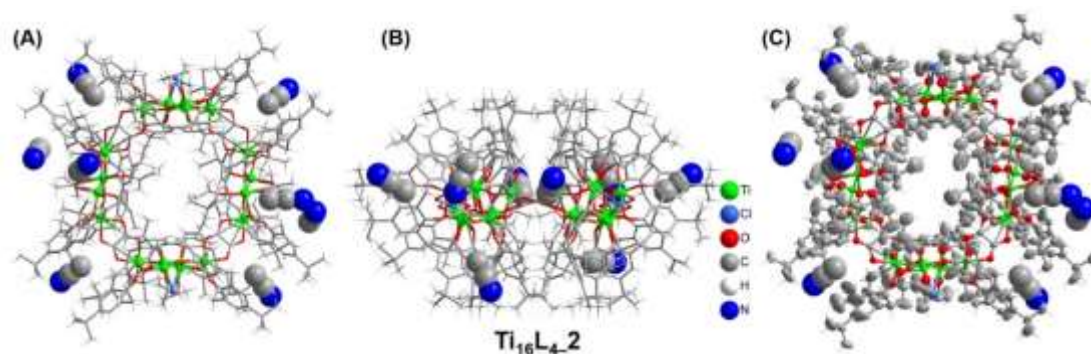


Figure S4. The molecular structure of $\text{Ti}_{16}\text{L}_4\mathbf{2}$. (a) and (a) The ball-and-stick view; (b) the ORTEP-style view.

The molecular formula of $\text{Ti}_{16}\text{L}_4\mathbf{2}$ was determined as $[\text{H}_4\text{Ti}_{16}\text{O}_8(\text{TBC}[8])_4(\text{C}_2\text{O}_4)_4(\text{Ac})_2\text{Cl}_2(\text{O}^i\text{Pr})_8]^{-2}\cdot 56\text{CH}_3\text{CN}$. Some highly disordered solvent molecules in the crystal structures were removed with the SQUEEZE program in PLATON, and its possible formula was proposed based on the SQUEEZE and TGA results. SCXRD analysis showed the position of some guest molecules for $\text{Ti}_{16}\text{L}_4\mathbf{2}$. Unlike $\text{Ti}_{16}\text{L}_4\mathbf{1}$, no $^i\text{PrOH}$ molecules were found inside the ring. Outside the macrocycle, there are acetonitrile molecules located at the cup mouth of the $\{\text{Ti}_4\text{O}_2(\text{TBC}[8])(\text{Ac})(\text{O}^i\text{Pr})_2\}$ units. No CH_3CN was found at the cup mouth of the $\{\text{Ti}_4\text{O}_2(\text{TBC}[8])(\text{Cl})(\text{O}^i\text{Pr})_2\}$ units. This may be due to the high electronegativity of Cl^- ions, which

is not conducive to the proximity of acetonitrile molecule. In addition, like $\text{Ti}_{16}\text{L}_4\text{-1}$, CH_3CN guest is also present in the small pockets formed by the two adjacent TBC[8].

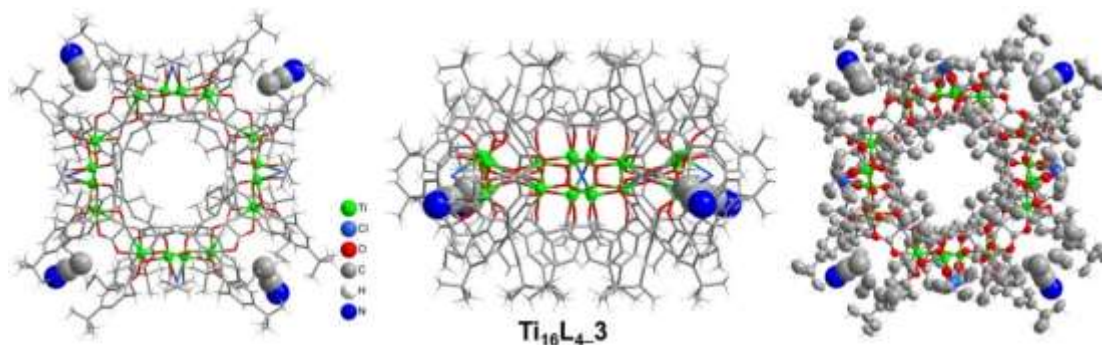


Figure S5. The molecular structure of $\text{Ti}_{16}\text{L}_4\text{-3}$. (a) and (a) The ball-and-stick view; (b) the ORTEP-style view.

The molecular formula of $\text{Ti}_{16}\text{L}_4\text{-3}$ was determined as $[\text{H}_4\text{Ti}_{16}\text{O}_8(\text{TBC}[8])_4(\text{C}_2\text{O}_4)_4\text{Cl}_4(\text{O}^i\text{Pr})_8]\cdot 40\text{CH}_3\text{CN}$. Some highly disordered solvent molecules in the crystal structures were removed with the SQUEEZE program in PLATON, and its possible formula was proposed based on the SQUEEZE and TGA results. SCXRD analysis showed the position of some guest molecules for $\text{Ti}_{16}\text{L}_4\text{-3}$. Outside the macrocycle, CH_3CN guest is present in the small pockets formed by the two adjacent TBC[8], but no guest molecules were found at the cup mouth of the four $\{\text{Ti}_4\text{O}_2(\text{TBC}[8])(\text{Cl})(\text{O}^i\text{Pr})_2\}$ units. This is consistent with the situation in $\text{Ti}_{16}\text{L}_4\text{-3}$.

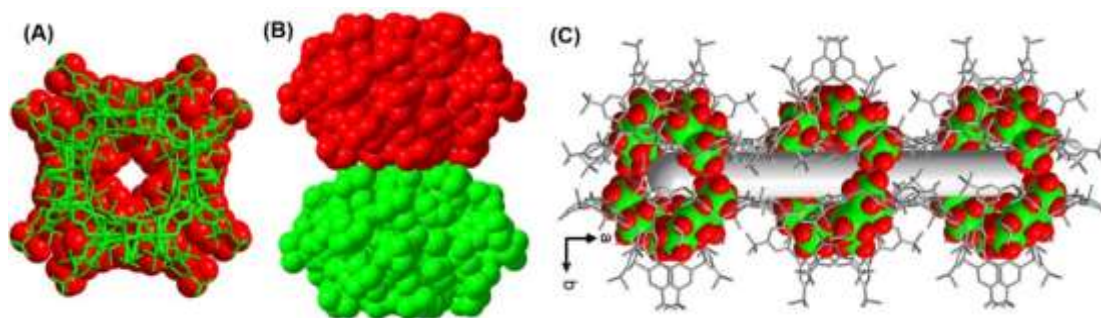


Figure S6. The as-formed nanotube in Ti_{16}L_4 .

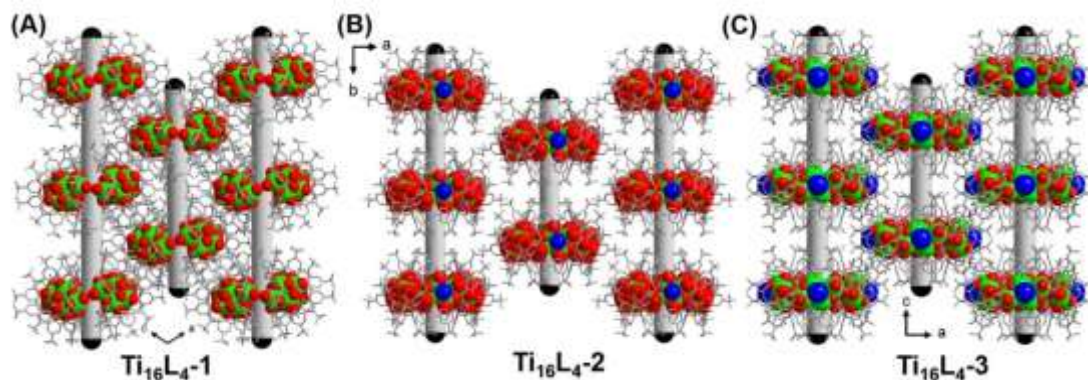


Figure S7. The adjacent nanotubes in Ti_{16}L_4 are interlaced with each other to avoid the spatial repulsion between the tert-butyl of the adjacent ring.

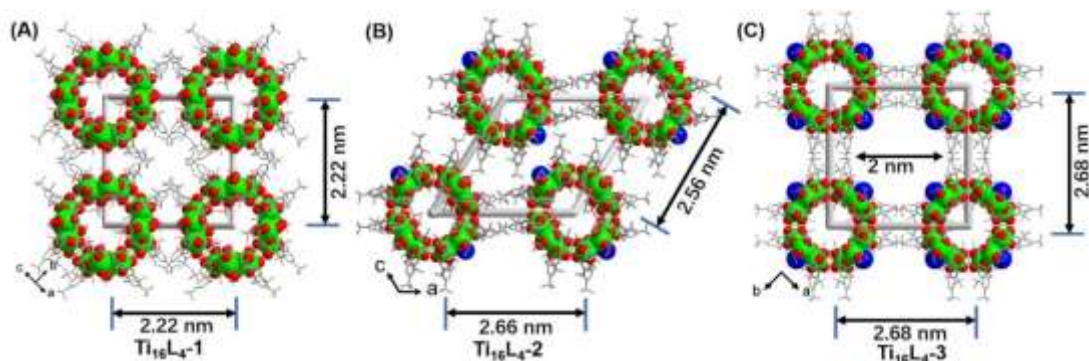


Figure S8. Three patterns of nanotubes arrangement in square array or hexagonal array.

Table S2: Crystallographic data of derived clusters of $Ti_{16}L_4$ obtained through Path I.

	Soaking the $Ti_{16}L_4-1$ in 1M formic acid solution for 24h	Soaking the $Ti_{16}L_4-1$ in 5M formic acid solution for 24 h	Soaking the $Ti_{16}L_4-2$ in 5M trifluoroacetic acid solution for 24h	Soaking the $Ti_{16}L_4-1$ in 5M chloroacetic acid solution for 24h	Soaking the $Ti_{16}L_4-1$ in 5M bromoacetic acid solution for 24h
Compounds	$Ti_{16}L_4-1(a)$	$Ti_{16}L_4-1/HFa(a)$	$Ti_{16}L_4-2/HTfa$	$Ti_{16}L_4-1/HCl_a$	$Ti_{16}L_4-1/HBra$
CCDC	2174432	2180762	2287667	2287668	2240657
Cryst. syst.	monoclinic	monoclinic	monoclinic	monoclinic	monoclinic
Space group	C2/c	C2/c	C2/c	C2/c	C2/c
Formula	$C_{380}H_{496}O_{95}Ti_{16}$	$C_{382}H_{479}N_3O_{80}Ti_{16}$	$C_{382}H_{450}F_{12}N_4O_{72}Ti_{16}$	$C_{380}H_{552}Cl_4O_{16}$	$C_{378}H_{448}Br_4O_{74}Ti_{16}$
F_w	7350.14	7159.05	7243.83	7980.38	7261.38
$a[\text{\AA}]$	38.100(2)	37.993(4)	54.372(7)	39.051(3)	39.278(7)
$b[\text{\AA}]$	33.157(2)	33.265(4)	20.162(2)	32.810(3)	32.838(6)
$c[\text{\AA}]$	37.2491(19)	37.218(4)	50.494(7)	37.614(3)	37.800(6)
$\beta[^\circ]$	113.291(2)	113.350(5)	121.984(4)	115.050(3)	115.147(5)
$V[\text{\AA}^3]$	43222(4)	43184(9)	46950(10)	43661(6)	44135(13)
Z	4	4	4	4	4
ρ_{calc}/cm^3	1.130	1.101	1.025	1.214	1.093
μ/mm^{-1}	1.981	1.960	1.823	2.162	2.186
F(000)	15552.0	15136.0	15224.0	16912.0	15200.0
2 θ range for data collection/ $^\circ$	4.394 to 102.69	4.752 to 110	4.886 to 90.208	4.718 to 84.988	3.186 to 96.354
Data/restraints/para meters	35504/446/2338	40988/559/2396	28404/2173/2 516	23005/917/24 81	42512/1936/2318
GooF	1.061	1.056	1.118	1.118	1.206
R1/wR2(I > 2 σ (I))	0.0750/0.2233	0.0920/0.2646	0.0902/0.2705	0.1329/0.3450	0.1387/0.3608
R1/wR2(all data)	0.1040/0.2420	0.1283/0.2941	0.1304/0.3036	0.1794/0.3742	0.1732/0.3810

Table S3: Crystallographic data of derived clusters of $Ti_{16}L_4$ obtained through Path II.

Conditions	Soaking the $Ti_{16}L_4-1$ in 5M NaOH solution for 30 min	Soaking the $Ti_{16}L_4-1/NaOH$ in formic acid solution for 30 min	Soaking the $Ti_{16}L_4-1/NaOH$ in 1M acetic acid solution for 30 min	Soaking the $Ti_{16}L_4-1/NaOH$ in 1M aminoacetic acid	Soaking the $Ti_{16}L_4-1/NaOH$ in 1M oxalic acid solution for 30 min	Soaking the $Ti_{16}L_4-1/NaOH$ in 1M glycolic acid for 30 min	Soaking the $Ti_{16}L_4-1/NaOH$ in 1M phosphoric acid
------------	---	--	---	--	---	--	---

Compounds	solution for 30 min						solution for 30 min
	Ti₁₆L₄-1/NaOH	Ti₁₆L₄-1/HF_a(b)	Ti₁₆L₄-1/HAc	Ti₁₆L₄-1/HAm_a	Ti₁₆L₄-1/HO_a	Ti₁₆L₄-1/HG_a	Ti₁₆L₄-1/H₃PO₄
CCDC	2174433	2174435	2174434	2240528	2174438	2174437	2240658
Cryst. syst.	monoclinic	monoclinic	monoclinic	monoclinic	monoclinic	monoclinic	monoclinic
Space group	C2/c	C2/c	C2/c	C2/c	C2/c	C2/c	C2/c
Formula	C ₃₆₆ H ₄₅₁ N ₃ Na ₈ O ₈ 5Ti ₁₆	C ₃₆₄ H ₄₈₈ Na ₄ O ₁₁₄ Ti ₁₆	C ₃₉₆ H ₅₆₈ Na ₂ O ₁₄₁ Ti ₁₆	C ₃₈₄ H ₄₅₆ Na ₄ O ₈₄ T i ₁₆	C ₃₆₈ H ₄₂₀ O ₇₆ Ti ₁₆	C ₃₇₂ H ₄₄₂ N ₂ O ₈₄ Ti ₁₆ 6	C ₃₆₀ H ₄₂₄ O ₇₁ Ti ₁₆
F _w	7202.24	7545.87	8396.85	7273.82	6825.42	7051.65	6873.37
a[Å]	38.447(2)	37.982(7)	39.095(9)	39.187(3)	39.32(4)	38.8238(16)	38.634(3)
b[Å]	32.9077(17)	33.195(6)	33.277(15)	33.088(2)	32.41(4)	32.5568(14)	32.619(3)
c[Å]	37.172(2)	36.904(7)	37.714(16)	37.420(3)	37.78(3)	37.8922(16)	37.291(3)
β[°]	114.933(2)	113.349(6)	114.899(9)	115.189(3)	115.25(3)	115.418(2)	114.837(2)
V[Å ³]	42646(4)	42718(14)	44508(30)	43905(6)	43259(3)	43536(74)	42646(6)
Z	4	4	4	4	4	4	Z
ρ _{calc} /cm ³	1.121	1.173	1.253	1.103	1.228	1.061	1.047
μ/mm ⁻¹	1.943	2.056	1.934	1.964	1.954	1.193	1.865
F(000)	15136.0	15944.0	11784.0	15336.0	17056.0	14528.0	14170.0
2θ range for data collection/°	4.758 to 104.634	4.784 to 96.476	4.694 to 96.42	6.098 to 104.68	4.718 to 84.636	4.702 to 103.078	4.758 to 94.958
Data/restraints/parameters	36171/151/2310	30448/606/2223	31835/407/2397	37451/388/2445	22518/536/2115	35703/375/2225	28360/369/2094
Goof	1.154	1.046	1.064	1.205	1.079	1.096	0.992
R1/wR2(I>2σ(I))	0.1112/0.3308	0.0929/0.2702	0.0924/0.2705	0.1148/0.3256	0.1595/0.3789	0.0810/0.2623	0.1242/0.3362
R1/wR2(all data)	0.1265/0.3440	0.1313/0.3040	0.1306/0.3031	0.1470/0.3510	0.2193/0.4372	0.0929/0.2729	0.1727/0.3708

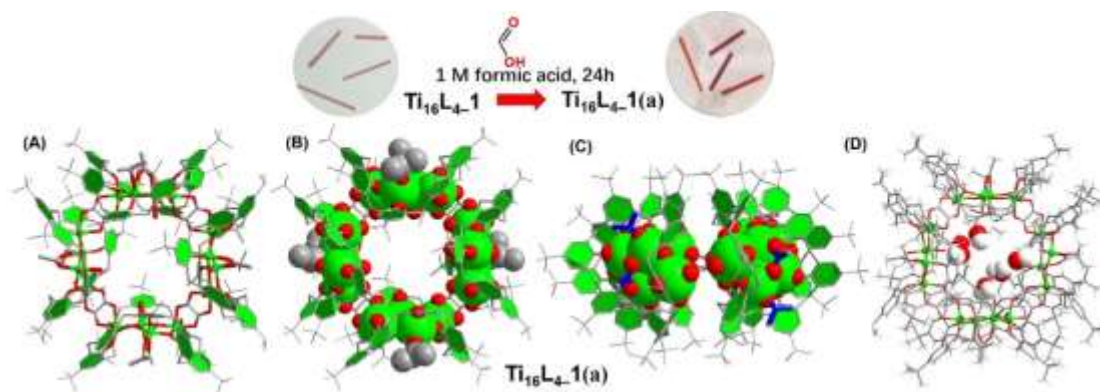


Figure S9. (A-C) Crystal structures of the **Ti₁₆L₄-1(a)**, emphasizing its nano-sized dimensions (top and side views). SCXRD analysis showed that the four internal ⁱPrO⁻ sites were replaced by H₂O molecules, but the four acetic acid sites and four internal ⁱPrO⁻ sites remained unchanged. (D) SCXRD analysis showed the position of some guest molecules for **Ti₁₆L₄-1(a)**. Because the crystal is immersed in water solution for a long time, the H₂O molecular occupies the inner space of the macrocycle.

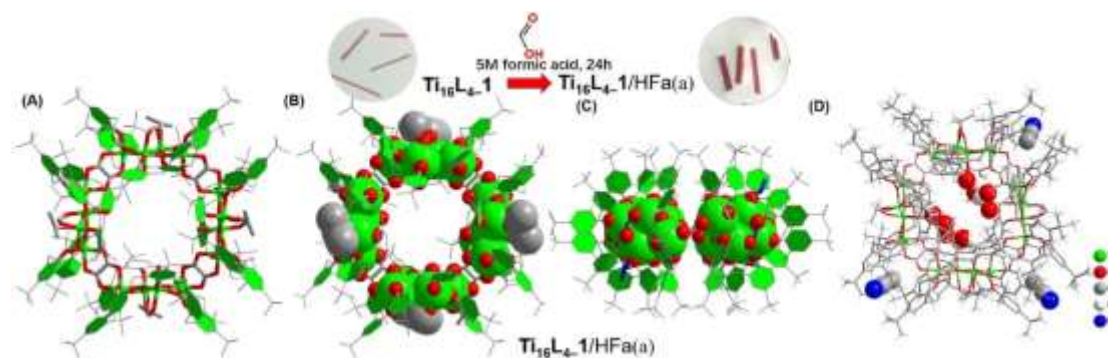


Figure S10. (A-C) Crystal structures of the $\text{Ti}_{16}\text{L}_4\text{-1}/\text{HF}a(a)$, emphasizing its nano-sized dimensions (top and side views). SCXRD analysis showed that four acetate sites were replaced by formate ligands, and four internal ${}^i\text{PrO}^-$ sites were replaced by H_2O molecules, but the four external ${}^i\text{PrO}^-$ sites remained unchanged. (D) SCXRD analysis showed the position of some guest molecules for $\text{Ti}_{16}\text{L}_4\text{-1}/\text{HF}a(a)$. The inner space of the macrocycle is occupied by H_2O molecules. No CH_3CN guest molecules were found at the cup mouth of the four $\{\text{Ti}_4\text{O}_2(\text{TBC}[8])\}$ units. However, in the small pockets formed by the two adjacent $\{\text{Ti}_4\text{O}_2(\text{TBC}[8])\}$ units, the CH_3CN guest is still existed.

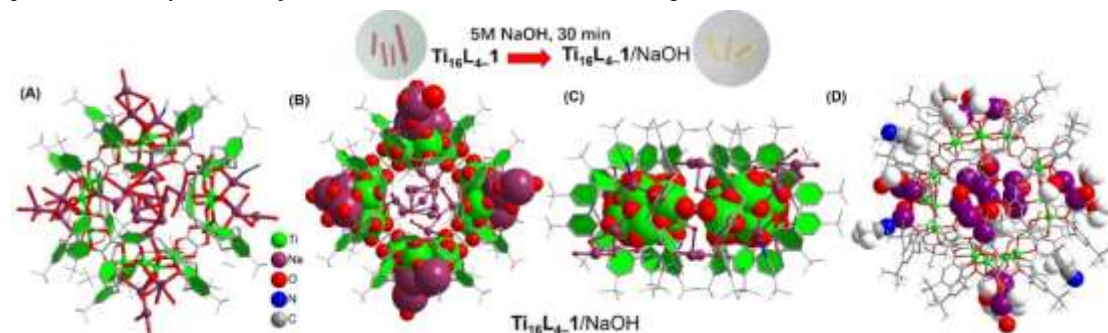


Figure S11. (A-C) Crystal structures of the $\text{Ti}_{16}\text{L}_4\text{-1}/\text{NaOH}$, emphasizing its nano-sized dimensions (top and side views). The surface acetate and ${}^i\text{PrO}^-$ ligands are fully exchanged by the OH^- ion; (D) SCXRD analysis showed the position of some guest molecules for $\text{Ti}_{16}\text{L}_4\text{-1}/\text{NaOH}$. Because the crystal is immersed in NaOH solution, and a large amount of Na^+ ions are embedded in the ring via OH^- bridging. The $\text{Ti}:\text{Na}$ ration in $\text{Ti}_{16}\text{L}_4\text{-1}/\text{NaOH}$ was confirmed to be about 2.07:1 by ICP-AES analysis, which is almost consistent with EDS results. Interestingly, in the small pockets formed by the two adjacent $\{\text{Ti}_4\text{O}_2(\text{TBC}[8])\}$ units, the CH_3CN guest is still existed. This position can be thought of as a molecular cage, firmly trapping CH_3CN molecules inside.

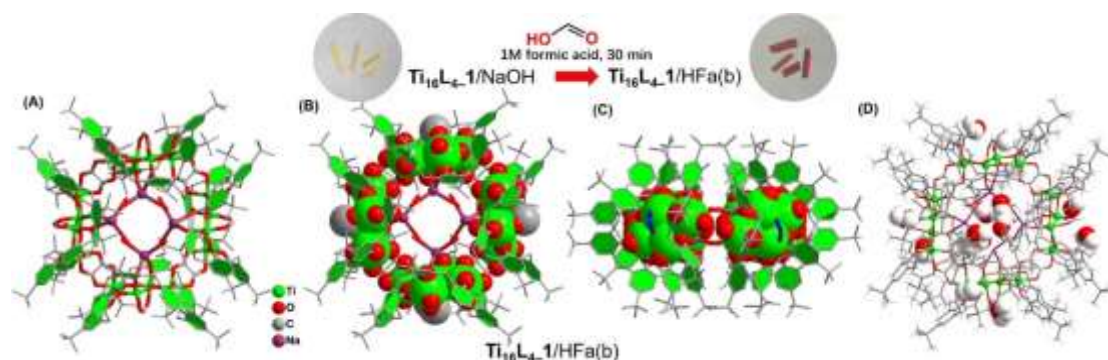


Figure S12. (A-C) Crystal structures of the $\text{Ti}_{16}\text{L}_4\text{-1}/\text{HF}a(b)$, emphasizing its nano-sized dimensions (top and side views). The four $\mu_2\text{-OH}^-$ sites were replaced by the formate ligands in the $\mu_2\text{-(O,O')}$ form again. The remaining eight OH^- sites are still occupied by water molecules. (D) SCXRD analysis showed the position of some guest molecules for $\text{Ti}_{16}\text{L}_4\text{-1}/\text{HF}a(b)$. Four Na^+ ions are embedded in the cluster through Fa^- bridging. The remaining space inside the macrocycle is occupied by H_2O molecules.



Figure S13. (A-C) Crystal structures of the $\text{Ti}_{16}\text{L}_4\text{-1}/\text{HBra}$, emphasizing its nano-sized dimensions (top and side views). SCXRD analysis showed that four acetic acid sites were replaced by bromoacetate ligands, and four internal ${}^i\text{PrO}^-$ sites were replaced by H_2O molecules, but the four external ${}^i\text{PrO}^-$ sites remained unchanged; (D) Because the crystal is immersed in water solution for a long time, the H_2O molecular occupies the inner space of the macrocycle.



Figure S14. (A-C) Crystal structures of the $\text{Ti}_{16}\text{L}_4\text{-1}/\text{HClA}$, emphasizing its nano-sized dimensions (top and side views). SCXRD analysis showed that four acetic acid sites were replaced by chloroacetate ligands, and four internal ${}^i\text{PrO}^-$ sites were replaced by H_2O , but the four external ${}^i\text{PrO}^-$ sites remained unchanged; (D) Because the crystal is immersed in water solution for a long time, the H_2O molecular occupies the inner space of the macrocycle.

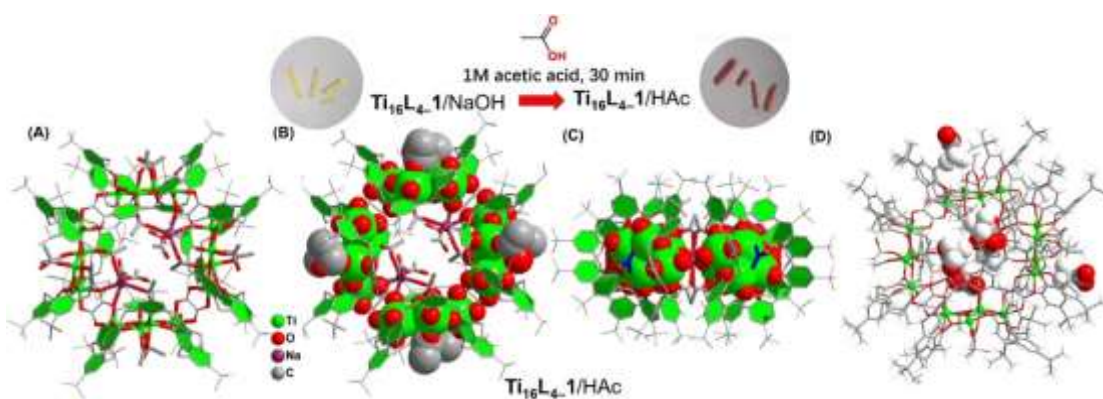


Figure S15. (A-C) Crystal structures of the $\text{Ti}_{16}\text{L}_4\text{-1}/\text{HAc}$, emphasizing its nano-sized dimensions (top and side views). All twelve OH^- sites were replaced by acetate ligands again. (D) SCXRD analysis showed the position of some guest molecules for $\text{Ti}_{16}\text{L}_4\text{-1}/\text{HAc}$. Two Na^+ ions are embedded in the cluster through acetate bridging, and four additional acetic acid molecules are embedded into the ring through coordination with Na^+ ions. No CH_3CN guest molecules are found outside the ring.

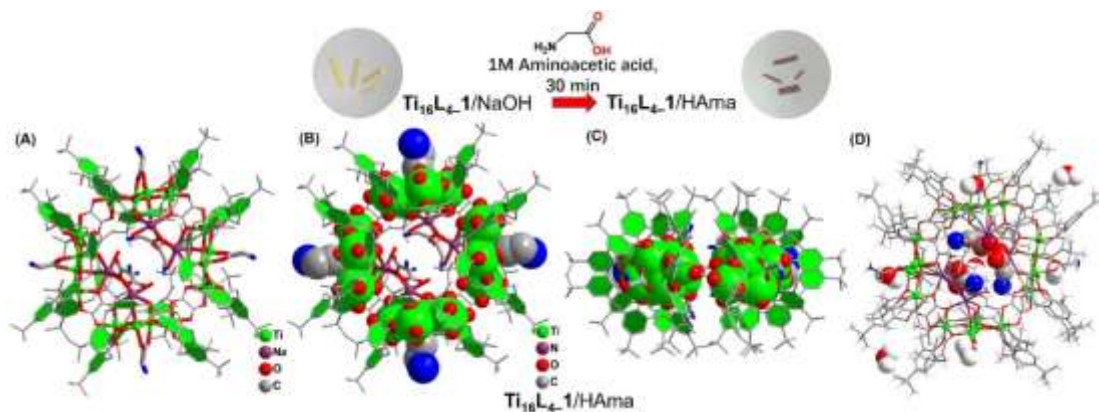


Figure S16. (A-C) Crystal structures of the $\text{Ti}_{16}\text{L}_4\text{-1}/\text{Hama}$, emphasizing its nano-sized dimensions (top and side views). The four $\mu_2\text{-OH}^-$ sites were replaced by the aminoacetate ligands in the $\mu_2\text{-(O,O)}$ form. The remaining eight OH^- sites are still occupied by water molecules; (D) SCXRD analysis showed the position of some guest molecules for $\text{Ti}_{16}\text{L}_4\text{-1}/\text{Hama}$. Four Na^+ ions are embedded in the cluster through acetate bridging, and four additional aminoacetic acid molecules are embedded into the ring through coordination with Na^+ ions. No CH_3CN guest molecules are found outside the ring.

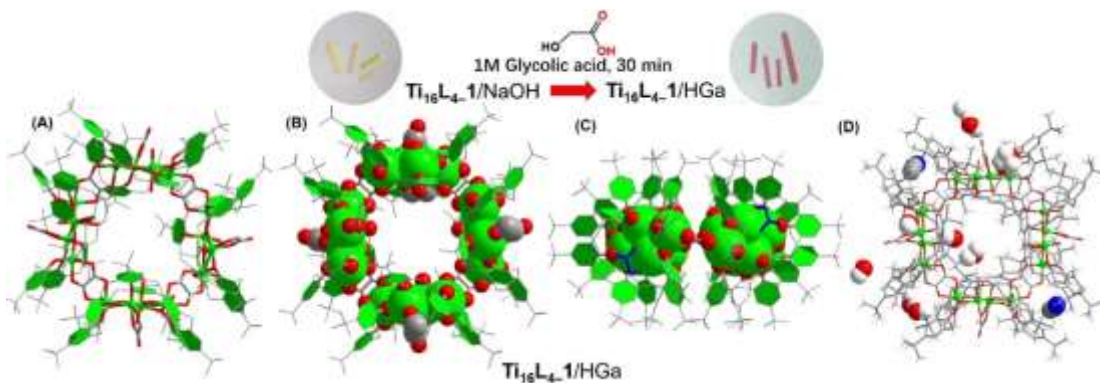


Figure S17. (A-C) Crystal structures of the $\text{Ti}_{16}\text{L}_4\text{-1}/\text{HGa}$, emphasizing its nano-sized dimensions (top and side views). Four oxalate ligands coordinate with the Ti_3 site in chelate-bidentate $\mu_1\text{-(O,O)}$ mode, while eight OH^- ions are coordinated with Ti_2 sites. (D) SCXRD analysis showed the position of some guest molecules for $\text{Ti}_{16}\text{L}_4\text{-1}/\text{HGa}$. No residual Na^+ ions were found in the structure. The H_2O molecular occupies the inner space of the macrocycle. In the small pockets formed by the two adjacent $\{\text{Ti}_4\text{O}_2(\text{TBC}[8])\}$ units, the CH_3CN guest is still existed.

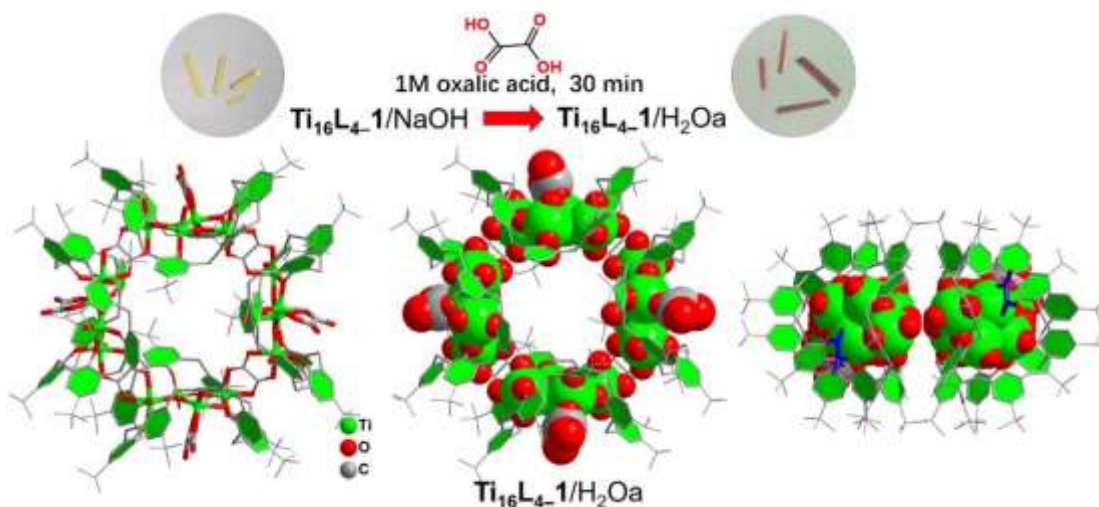


Figure S18. Crystal structures of the $\text{Ti}_{16}\text{L}_4\text{1}/\text{H}_2\text{O}$, emphasizing its nano-sized dimensions (top and side views). Four glycolate ligands coordinate with the Ti3 site in chelate-bidentate μ_1 -(O,O) mode, while eight OH^- ions are coordinated with Ti2 sites. Due to the weak diffraction data of the crystal, we have not been able to determine the position of the guest molecules.

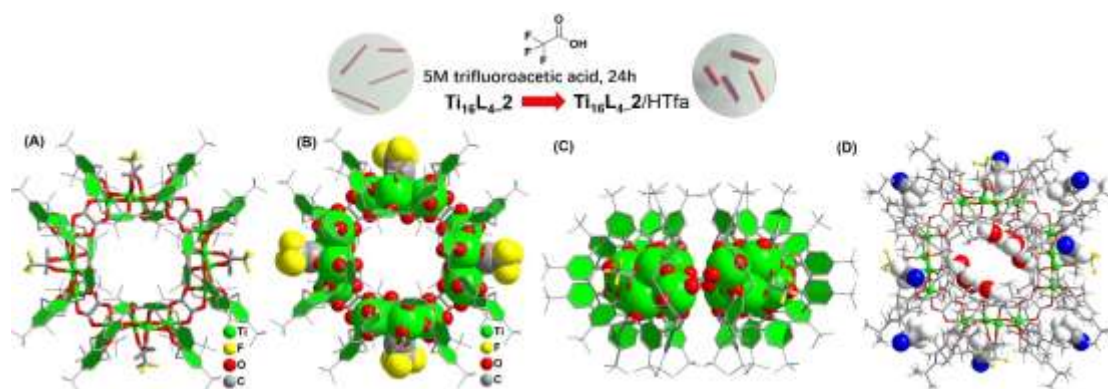


Figure S19. (A-C) Crystal structures of the $\text{Ti}_{16}\text{L}_4\text{2}/\text{HTfa}$, emphasizing its nano-sized dimensions (top and side views). SCXRD analysis showed that four acetic acid sites were replaced by trifluoroacetate, and four internal ${}^i\text{PrO}^-$ sites were replaced by H_2O , but the four external ${}^i\text{PrO}^-$ sites remained unchanged; (D) Because the crystal is immersed in water solution for a long time, the H_2O molecular occupies the inner space of the macrocycle.

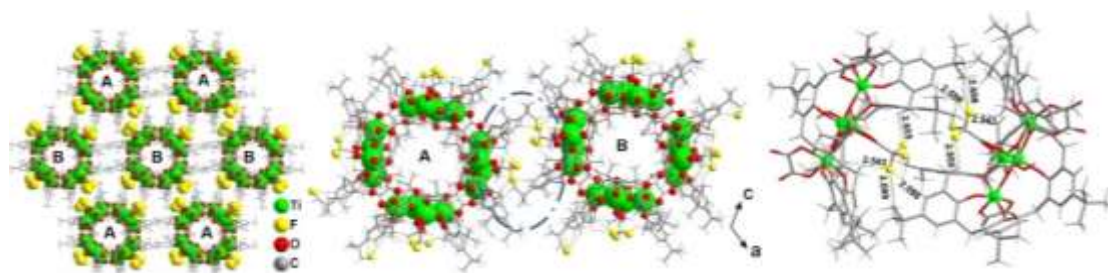


Figure S20. The hexagonal array of the nanotube in $\text{Ti}_{16}\text{L}_4\text{2}/\text{HTfa}$. Illustration of the H bonds between two interlocked clusters of $\text{Ti}_{16}\text{L}_4\text{2}/\text{HTfa}$.

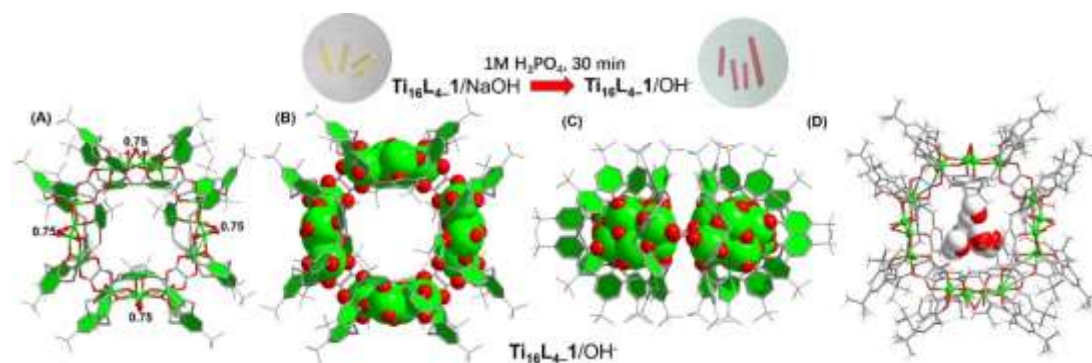


Figure S21. (A-C) Crystal structures of the $\text{Ti}_{16}\text{L}_4\text{1}/\text{OH}^-$, emphasizing its nano-sized dimensions (top and side views). SXRD showed that 12 unstable sites were still occupied by OH^- ions and H_2O molecules, and all Na^+ ions were detached from the structure; (D) SCXRD analysis showed the position of some guest molecules for $\text{Ti}_{16}\text{L}_4\text{1}/\text{OH}^-$. The H_2O molecular occupies the inner space of the macrocycle. No CH_3CN guest molecule was found after two exchanges in the acid-base.

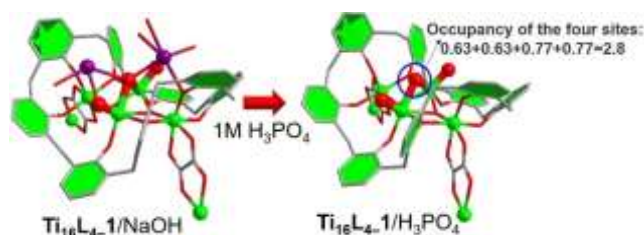


Figure 22. The crystals obtained by soaking $\text{Ti}_{16}\text{L}_4\text{-1}/\text{NaOH}$ in H_3PO_4 . Only the $\{\text{Ti}_4\text{-TBC}[8]\}$ subunit is given here. Notably, structural refinements indicate that the proportion of each $\mu_2\text{-O}$ site is only 0.75, and these four μ_2 -bridging fashion sites have a total of three OH ions. This means that after two ligand exchanges, one of the four μ_2 -bridging sites on the cluster is eventually deleted.

3. Powder X-ray diffraction

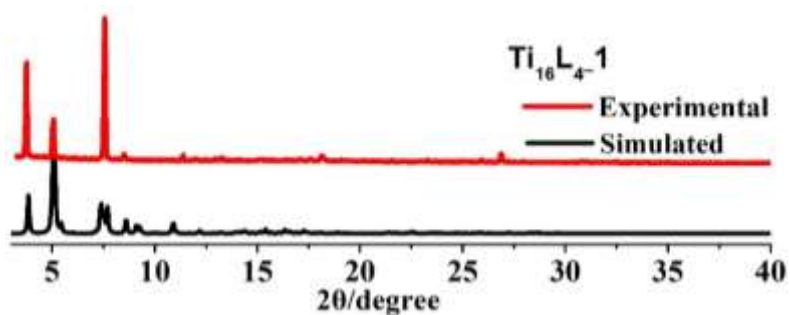


Figure S23. The XRD pattern of $\text{Ti}_{16}\text{L}_4\text{-1}$.

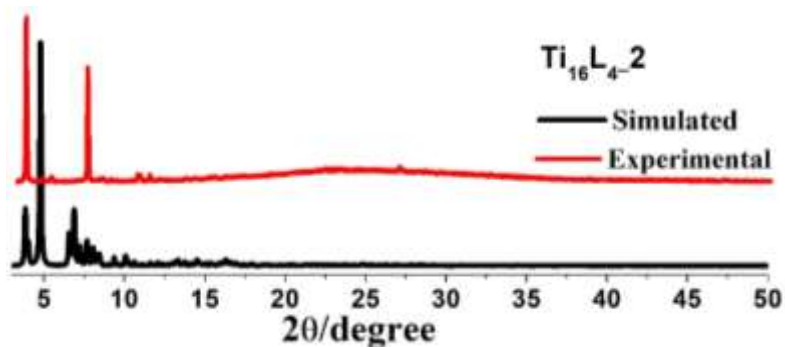


Figure S24. The XRD pattern of $\text{Ti}_{16}\text{L}_4\text{-2}$.

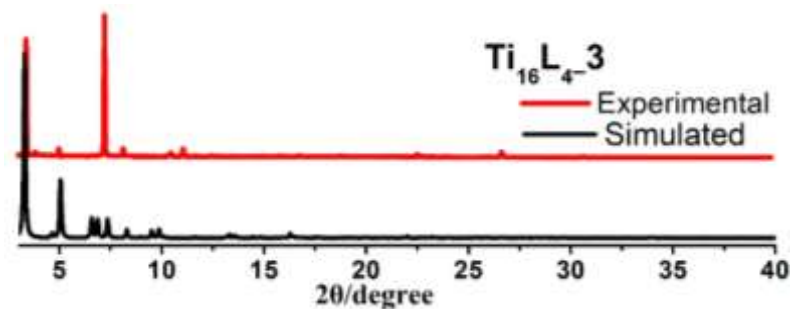


Figure S25. The XRD pattern of $\text{Ti}_{16}\text{L}_4\text{-3}$.

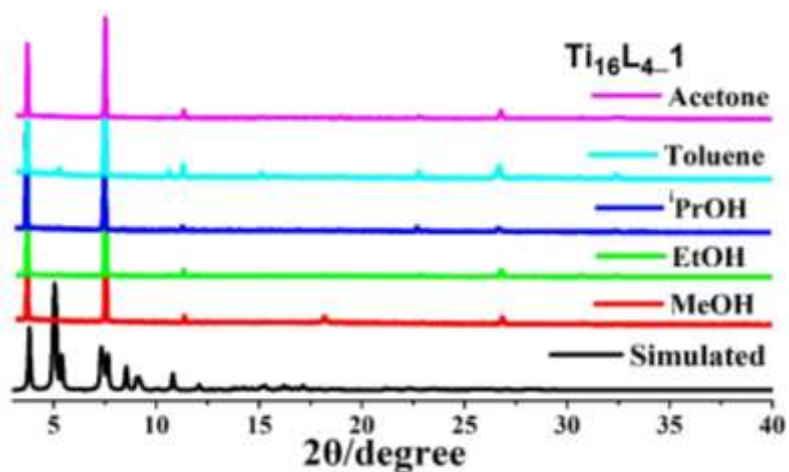


Figure S26. XRD patterns of $Ti_{16}L_{4-1}$ treated in different organic solvents at room temperature for one week.

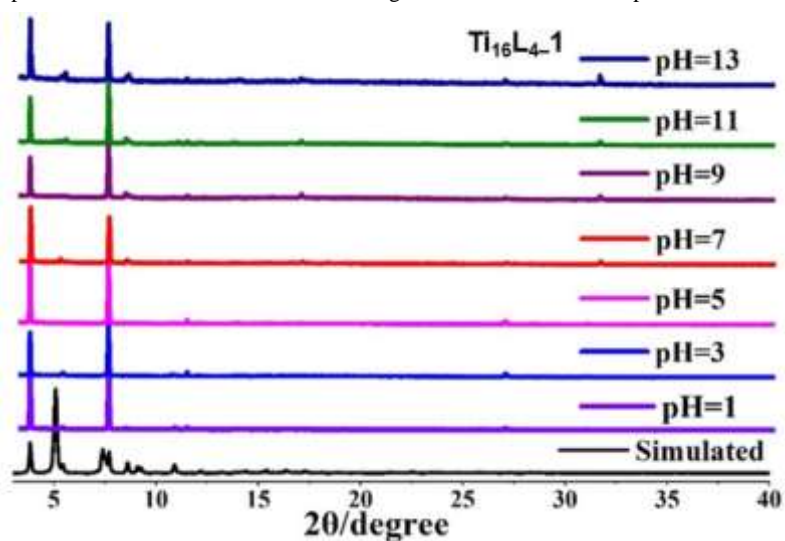


Figure S27. XRD patterns of $Ti_{16}L_{4-1}$ treated in different pH solutions at room temperature for 24 hours.

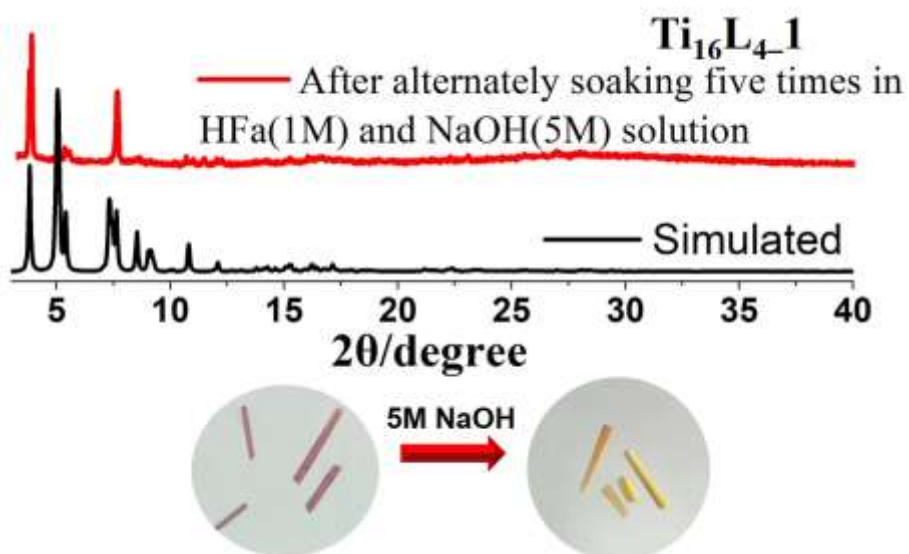


Figure S28. XRD patterns of $Ti_{16}L_{4-1}$ after alternating soaking in 5M NaOH and 1M HFa solution for five times. After five times of alternating soaking, the crystal is still firm and the color can obviously change between yellow and red.



Figure S29. The diffraction images of the crystal of **Ti₁₆L₄₋₁** after alternating soaking in 5M NaOH and 1M HFa solution for five times.

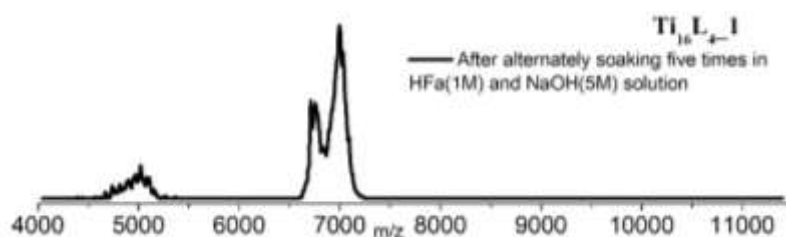


Figure S30. The diffraction images of the crystal of **Ti₁₆L₄₋₁** after alternating soaking in 5M NaOH and 1M HFa solution for five times.

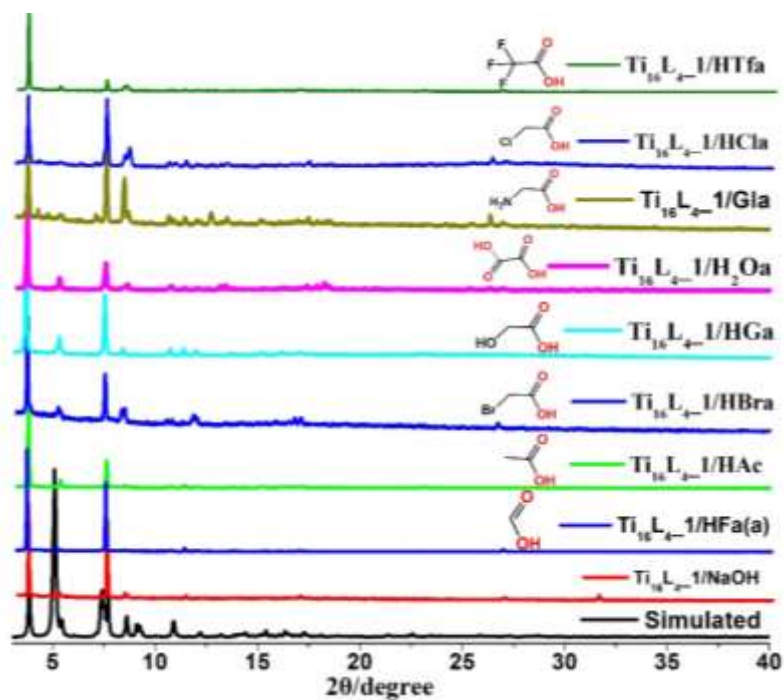


Figure S31. XRD patterns of the derived clusters of **Ti₁₆L₄₋₁** through post substitution methods.

4. XPS Measurement

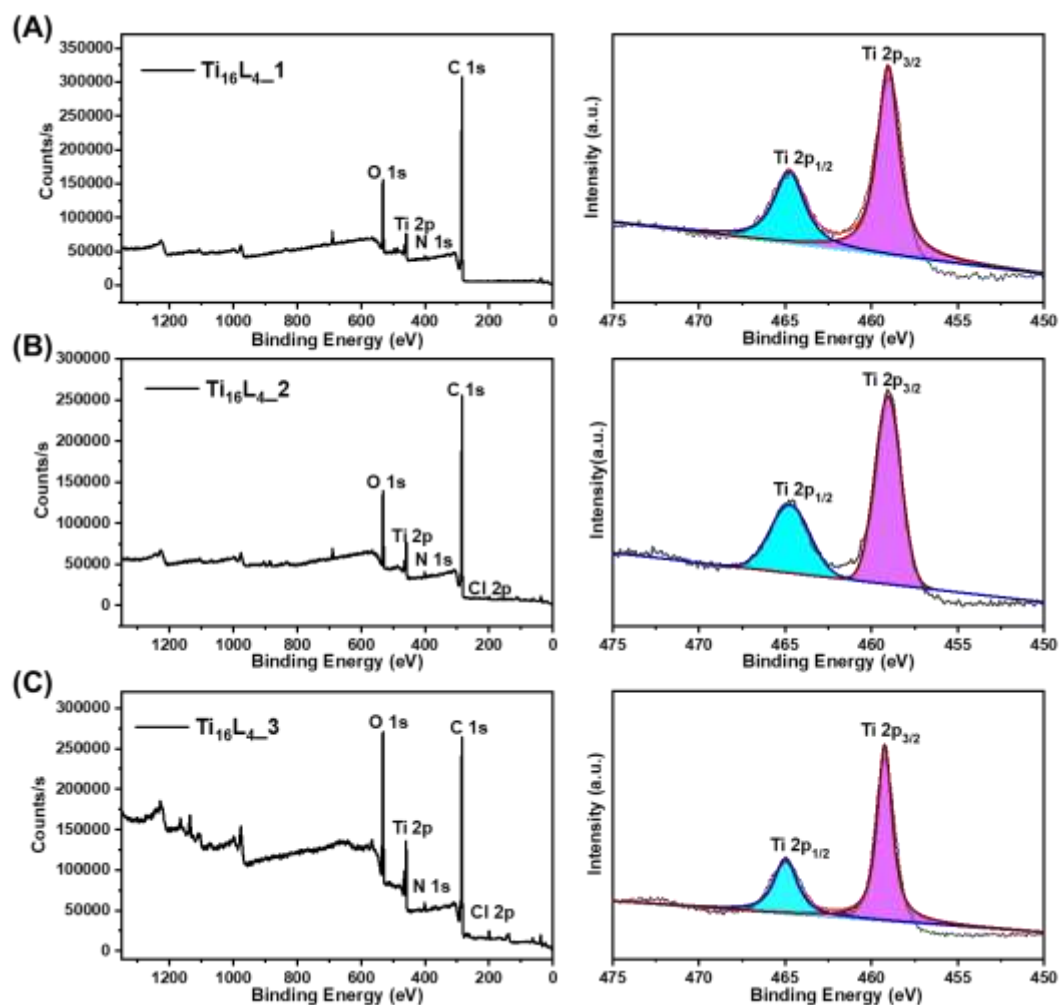


Figure S32. XPS Measurements for Ti_{16}L_4 . The presence of Ti^{4+} has been verified by the XPS analysis. In the case of $\text{Ti}_{16}\text{L}_{4-1}$, the Ti 2p spectrum exhibits distinct $\text{Ti } 2p^{1/2}$ (ca. 464.9 eV) and $\text{Ti } 2p^{3/2}$ (ca. 459.0 eV) regions, showing a binding energy difference of 5.9 eV. This discrepancy indicates the presence of Ti^{4+} . In the XPS spectra of $\text{Ti}_{16}\text{L}_{4-2}$ and $\text{Ti}_{16}\text{L}_{4-3}$, shifts in the binding energy peak of Ti are observed, attributed to ligand modifications.

5. TG Measurement

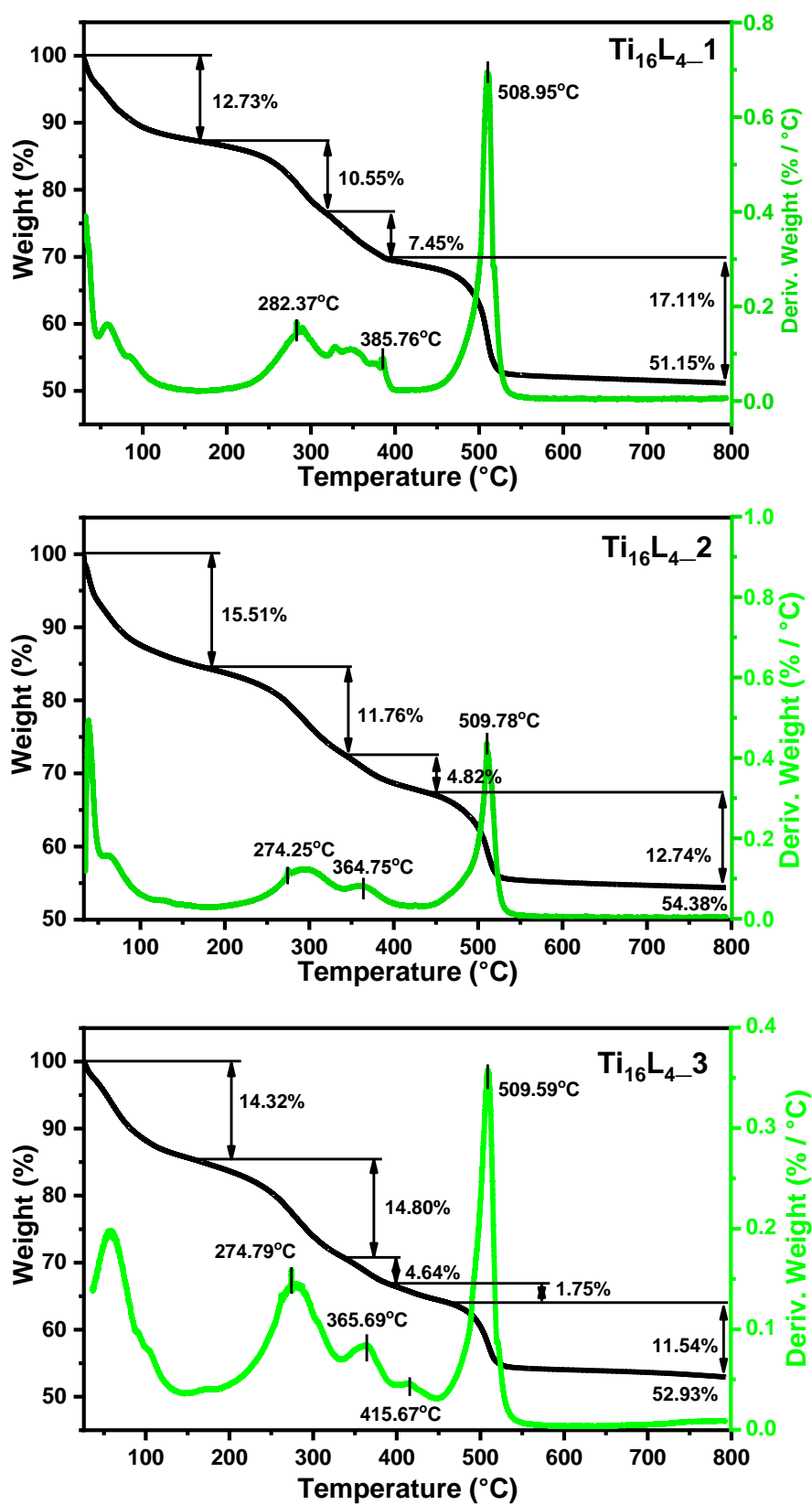


Figure S33. TGA curve of Ti₁₆L₄₋₁, Ti₁₆L₄₋₂ and Ti₁₆L₄₋₃.

6. IR Spectra

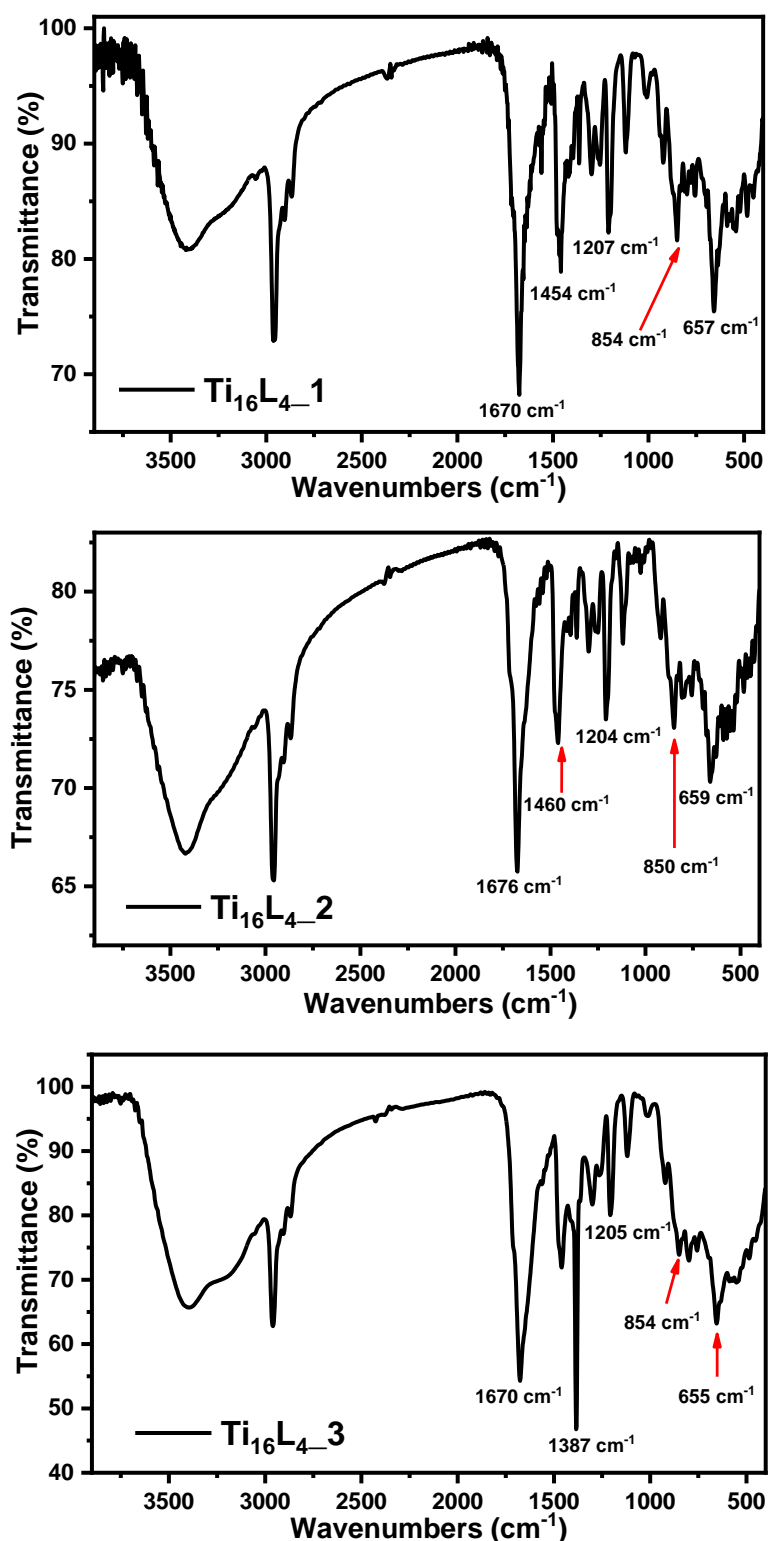


Figure S34. IR spectra of crystal samples of Ti_{16}L_4 -1, Ti_{16}L_4 -2 and Ti_{16}L_4 -3. In the high wavenumber region, the aborad absorption bands from 3700 to 3200 cm^{-1} stem from the $\nu(\text{O-H})$ stretching mode of $-\text{OH}$ groups or water molecules. The weak absorption bands at 3000–2800 cm^{-1} can be ascribed to the stretching vibration modes of C–H bonds in aromatic rings and tert butyl group. The characteristic stretching vibrations $\nu(\text{CO}_2^-)$ of in carboxylic groups and $\nu(\text{C}=\text{C})$ in benzene rings are overlapped from 1600 cm^{-1} to 1400 cm^{-1} . The characteristic bands of Ti–O–C and Ti–O–Ti appears in the ranges of 1000–1200 and 700–800 cm^{-1} , respectively.¹⁻²

Reference

1. Zhang, G., Hou, J., Li, M., Tung, C., Wang, Y., Counteranion-Stabilized Titanium(IV) Isopolyoxocationic Clusters Isolated from Water. *Inorg. Chem.* 2016, **55**, 4704-4709.
2. Zhang, G., Liu, C., Long, D., Cronin, L., Tung, C., Wang, Y., Water-Soluble Pentagonal-Prismatic Titanium-Oxo Clusters. *J. Am. Chem. Soc.* 2016, **138**, 11097–11100.

7. Energy Dispersive X-ray (EDX) Spectroscopic Analysis

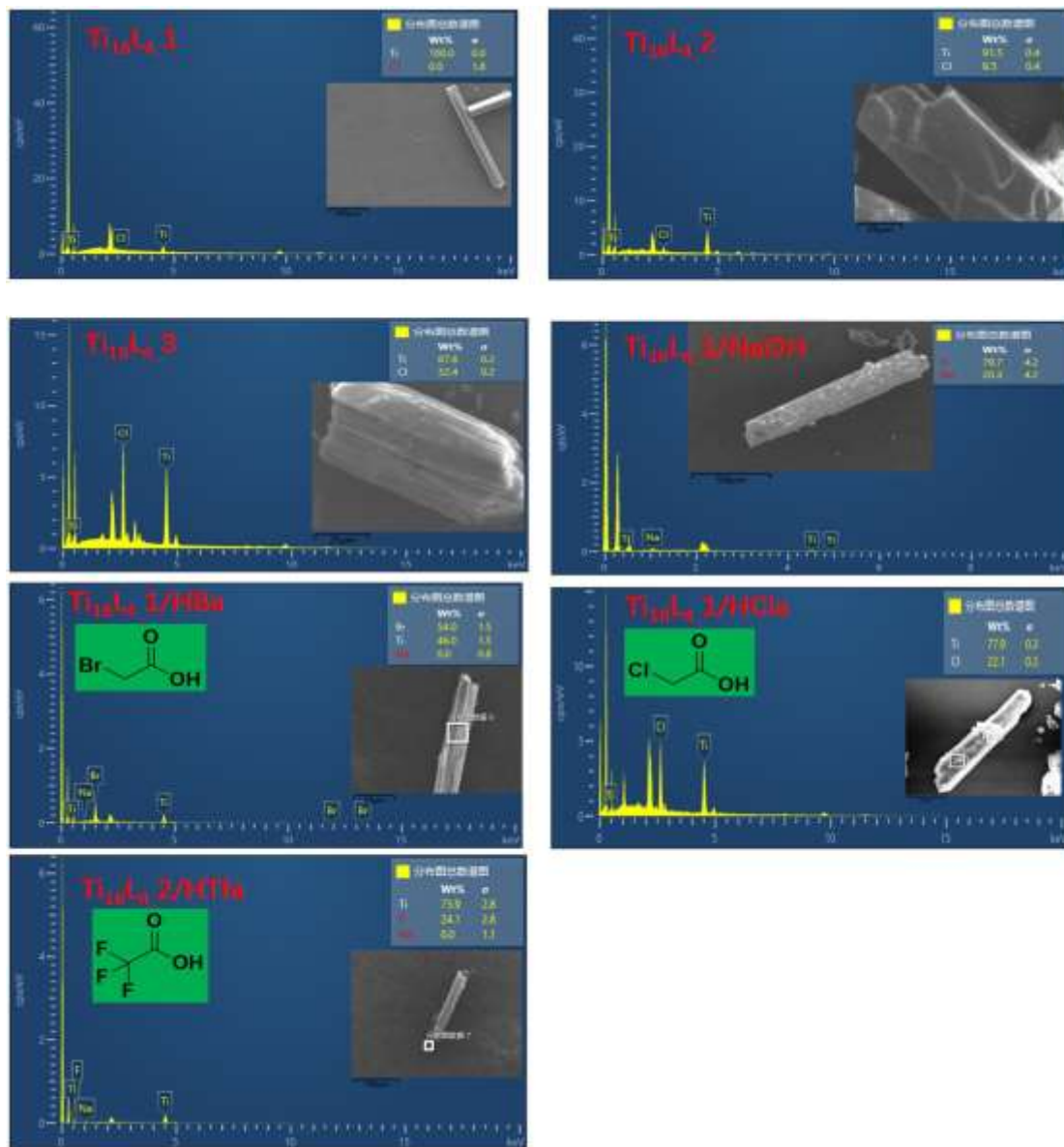


Figure S35. The EDS patterns of $\text{Ti}_{16}\text{L}_4\text{-1}$, $\text{Ti}_{16}\text{L}_4\text{-2}$, $\text{Ti}_{16}\text{L}_4\text{-3}$, $\text{Ti}_{16}\text{L}_4\text{-1/NaOH}$, $\text{Ti}_{16}\text{L}_4\text{-1/HBa}$, $\text{Ti}_{16}\text{L}_4\text{-1/HCl}$ and $\text{Ti}_{16}\text{L}_4\text{-2/HTfa}$. The presence of Cl^- ions in $\text{Ti}_{16}\text{L}_4\text{-2}$ and $\text{Ti}_{16}\text{L}_4\text{-3}$, Na ions in $\text{Ti}_{16}\text{L}_4\text{-1/NaOH}$, Br in $\text{Ti}_{16}\text{L}_4\text{-1/HBa}$, Cl in $\text{Ti}_{16}\text{L}_4\text{-1/HCl}$, and F in $\text{Ti}_{16}\text{L}_4\text{-2/HTfa}$ can be demonstrated by EDS.

8. CO₂ Adsorption

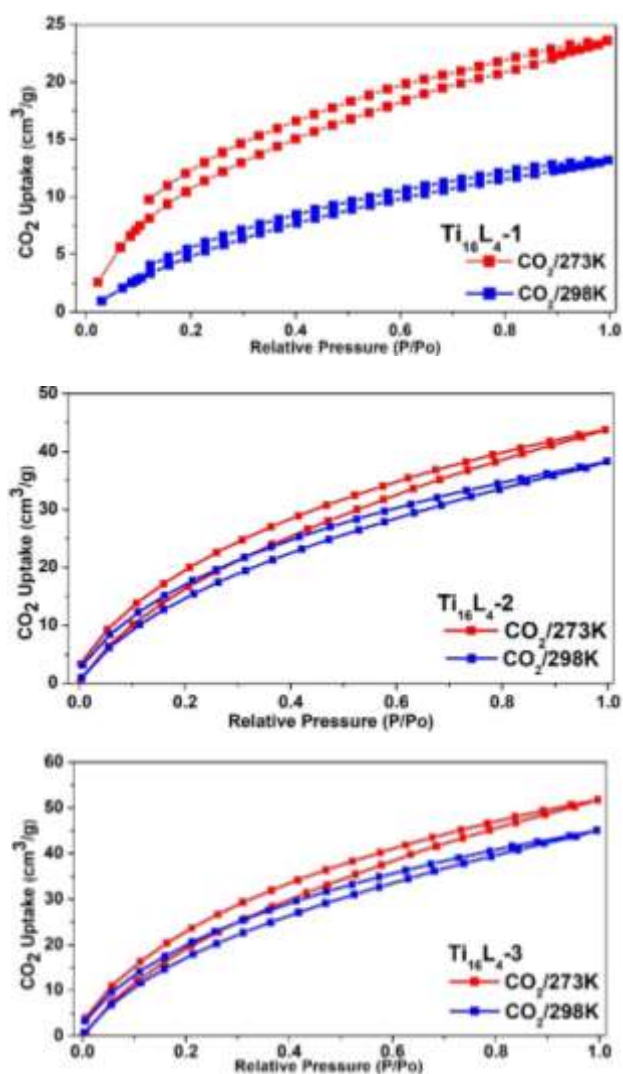
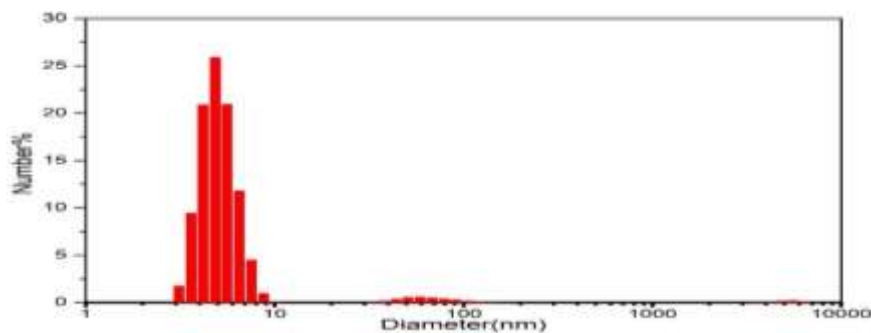


Figure S36. CO₂ adsorption and desorption isotherms of Ti₁₆L₄-1, Ti₁₆L₄-2 and Ti₁₆L₄-3 at 273 K (red) and 298 K (blue).

9. Dynamic Light Scattering Measurement



Dynamic light scattering (DLS) measurement is performed on a Malvern Zetasizer 1000HSA. The sample of Ti₁₆L₄-1 was dissolved in chloroform solution by ultrasonic dispersion. The solution was centrifuged. The clear solution was sucked out and placed in a quartz cuvette for measurement. In the range of 1-1000 nm, only one size distribution is observed with an average diameter of 4.2 nm, which matches the size of the cage (~3.0 nm) and verifies the existence of the cluster molecules in solution.

Figure S37. DLS of Ti₁₆L₄-1 in chloroform solution.

10. Wettability of $Ti_{16}L_4$ Rings

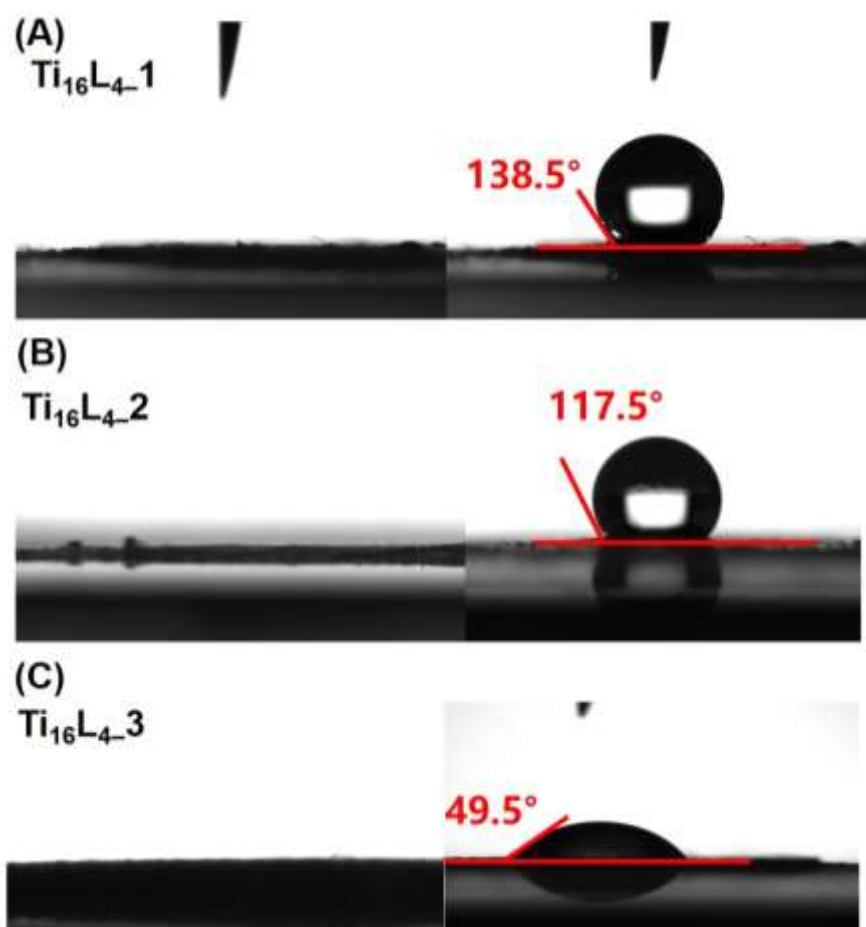


Figure S38. Contact angle patterns for $Ti_{16}L_4$ 1/2/3. The contact angles measured on as-synthesized powder samples of $Ti_{16}L_4$ 1/2/3 were 138.5°, 117.5° and 49.5°, respectively.

11. Photocatalysis

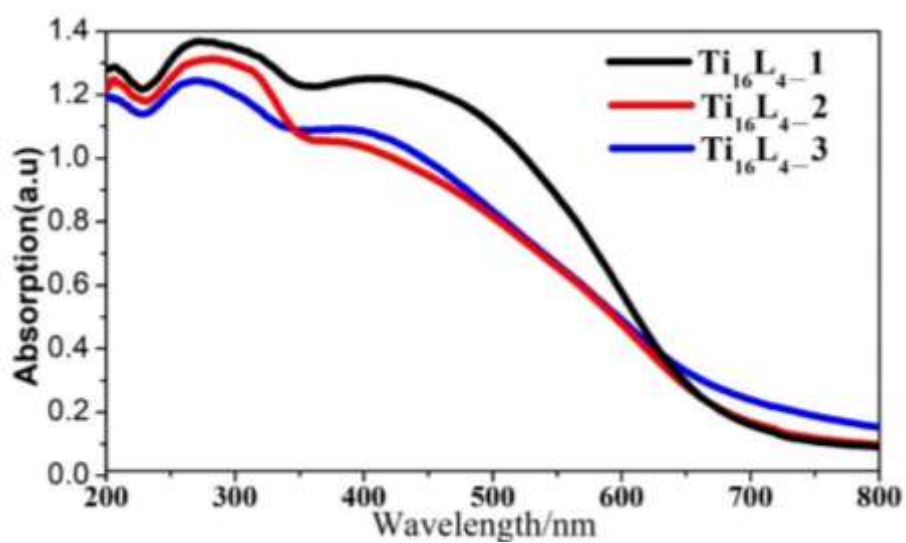


Figure S39. Solid state UV-Vis spectra of $Ti_{16}L_4$ 1/2/3.

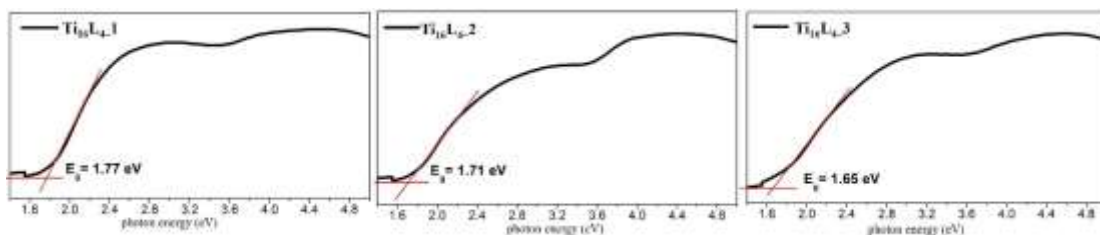


Figure S40. Tauc plot of Ti_{16}L_4 -1/2/3 derived from UV-vis spectra.

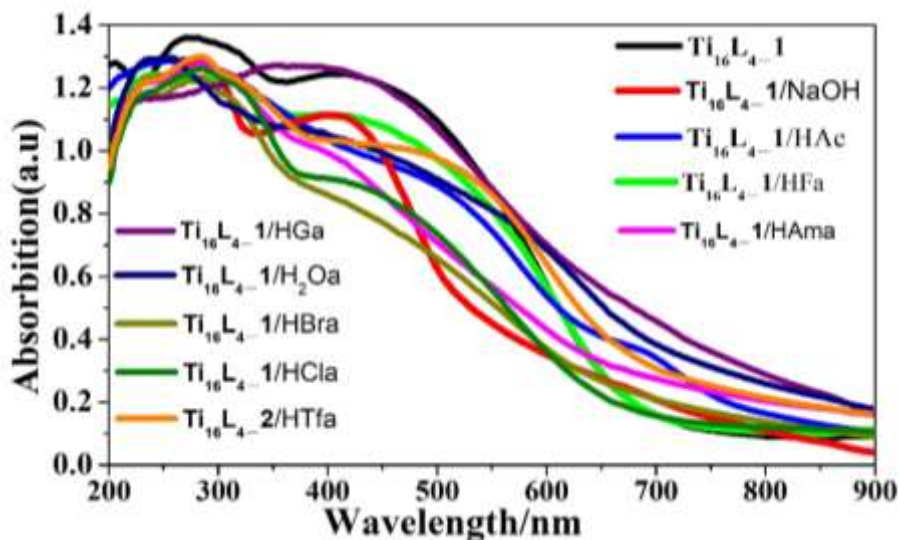


Figure S41. Solid state UV-Vis spectra of the derived Ti_{16}L_4 .

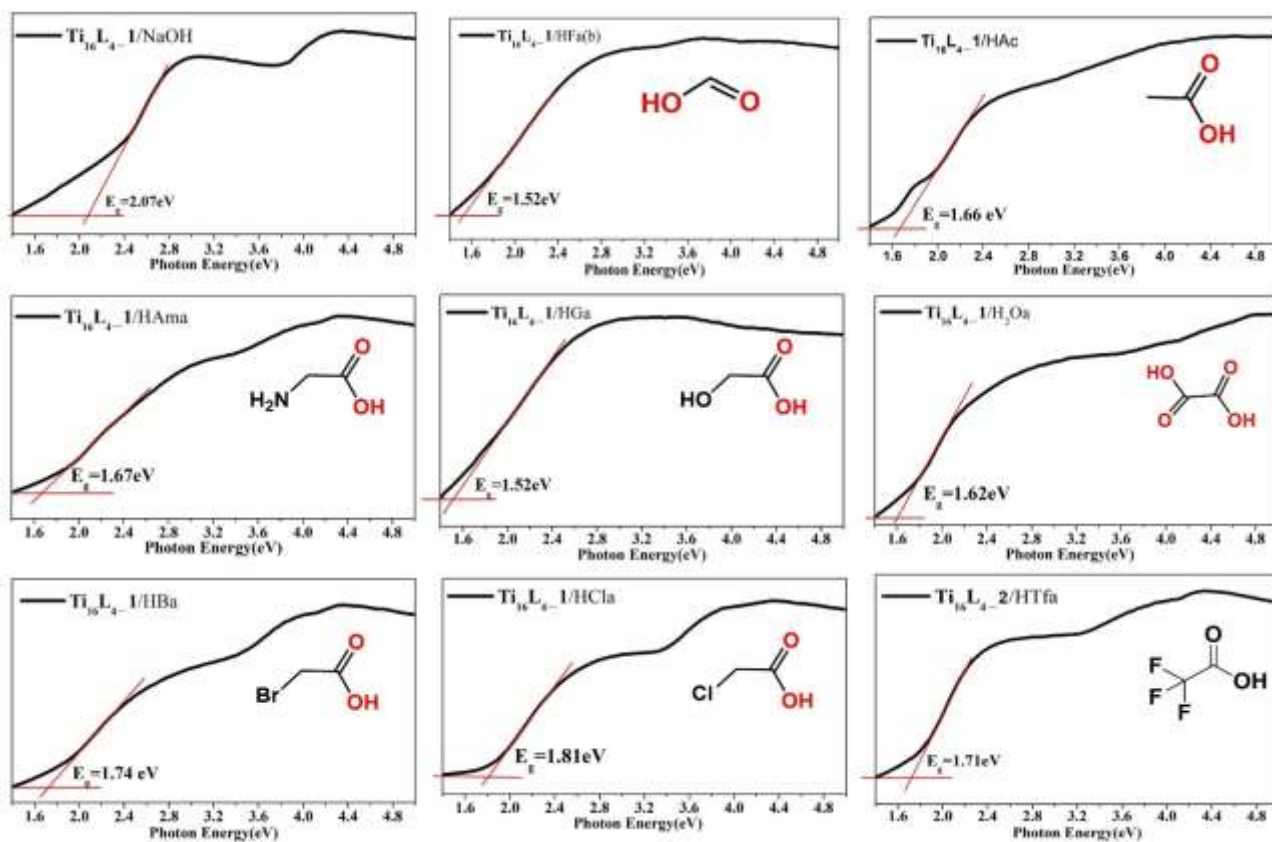


Figure S42. Tauc plot of the derived cluster of Ti_{16}L_4 -1 derived from UV-vis spectrum.

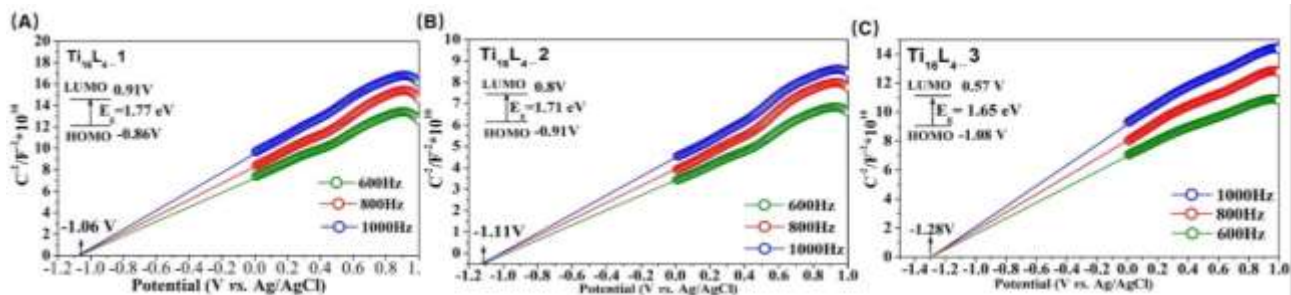


Figure S43. Mott-Schottky plots for Ti_{16}L_4 -1/2/3 in 0.2 M Na_2SO_4 aqueous solution. Insets are the energy diagrams of the HOMO and LUMO levels.

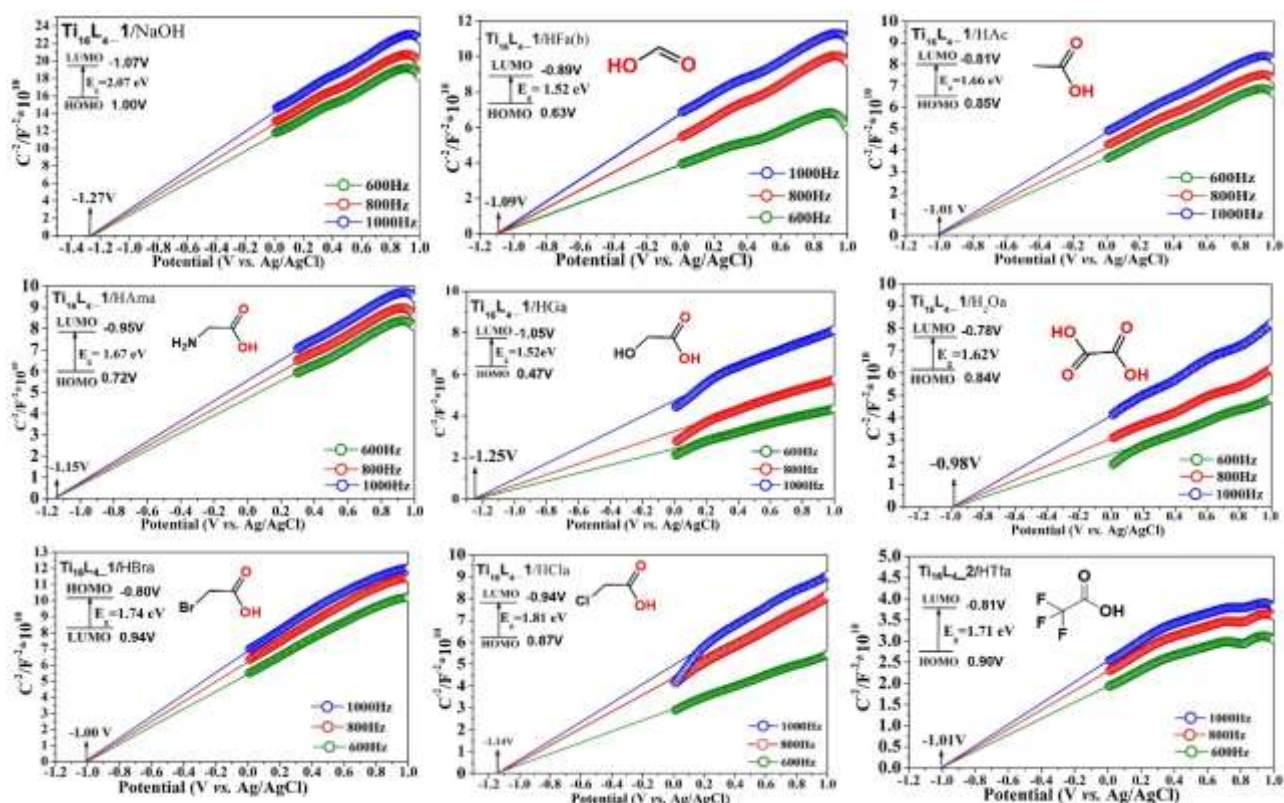


Figure S44. Mott-Schottky plots for the derived cluster of Ti_{16}L_4 -1 in 0.2 M Na_2SO_4 aqueous solution. Insets are the energy diagrams of the HOMO and LUMO levels.

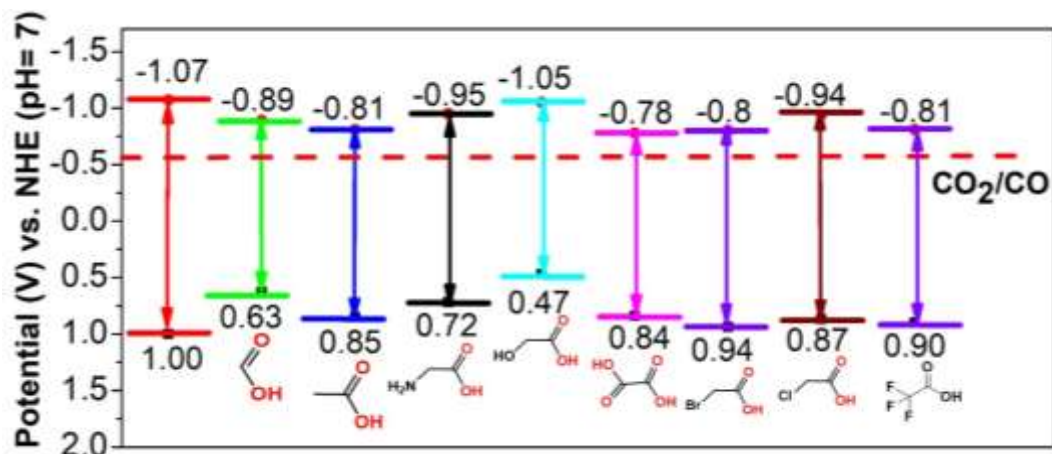


Figure S45. Band structure diagram for the derived cluster of Ti_{16}L_4 .



Figure S46. The picture of photocatalytic reactor.

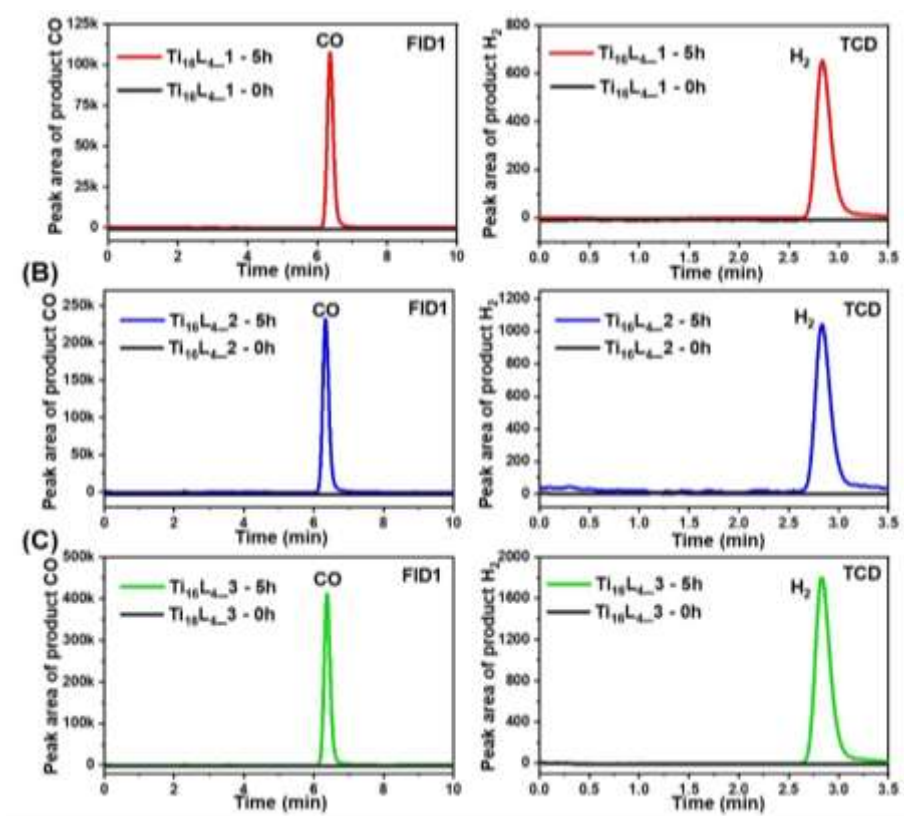


Figure S47. GC analysis of the gaseous reaction products for Ti₁₆L₄_1/2/3 by using the FID and TCD.

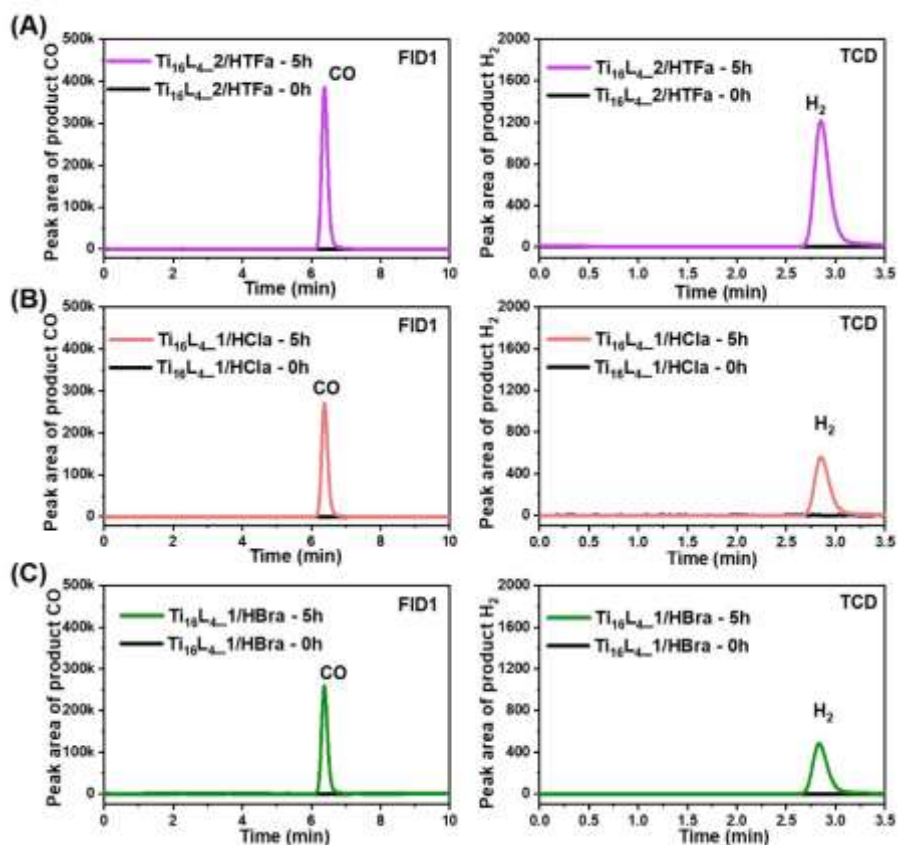


Figure S48. GC analysis of the gaseous reaction products for $\text{Ti}_{16}\text{L}_4\text{-2/HTFa}$, $\text{Ti}_{16}\text{L}_4\text{-1/HClA}$ and $\text{Ti}_{16}\text{L}_4\text{-2/HBra}$ by using the FID and TCD.

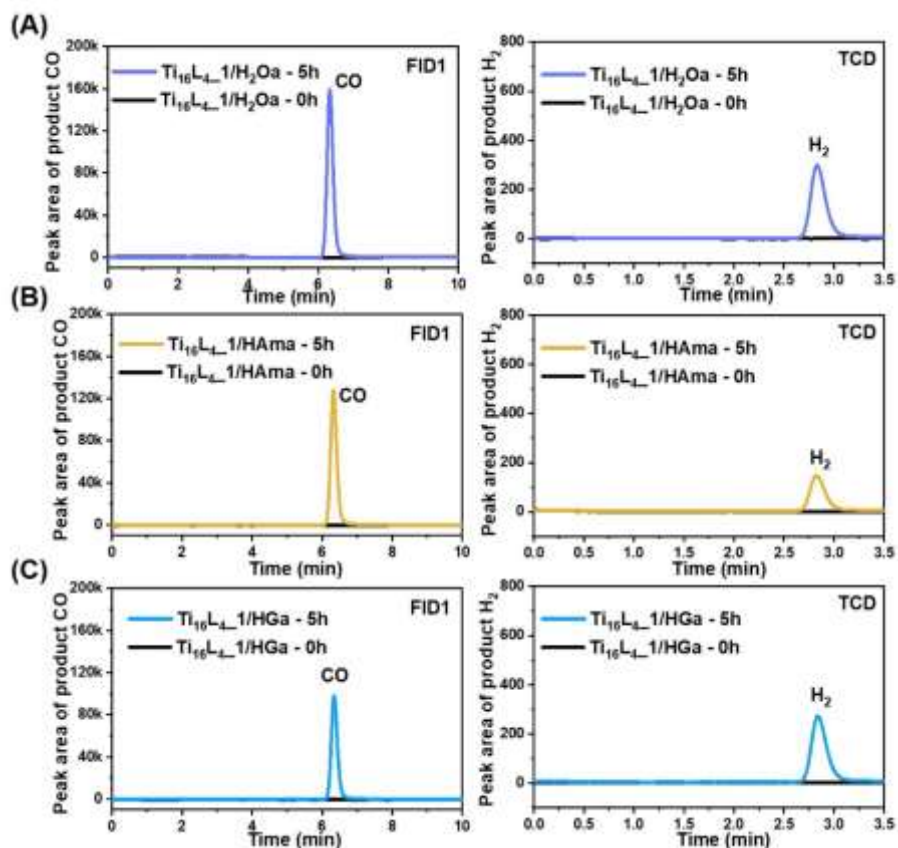


Figure S49. GC analysis of the gaseous reaction products for $\text{Ti}_{16}\text{L}_4\text{-1}/\text{H}_2\text{Oa}$, $\text{Ti}_{16}\text{L}_4\text{-1}/\text{Hama}$ and $\text{Ti}_{16}\text{L}_4\text{-1}/\text{HGa}$ by using the FID and TCD.

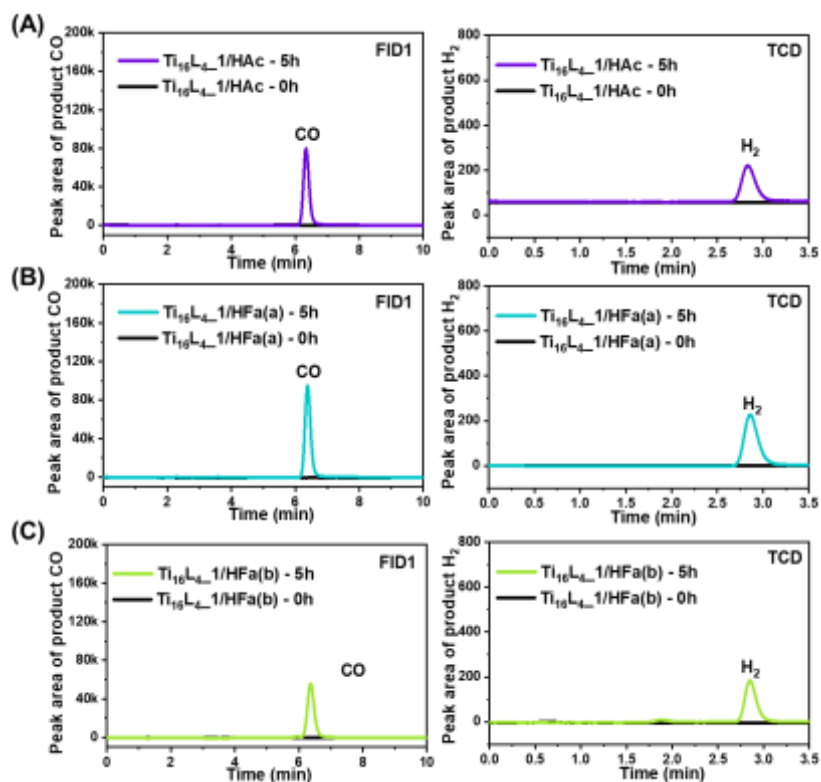


Figure S50. GC analysis of the gaseous reaction products for $\text{Ti}_{16}\text{L}_4\text{-1}/\text{HAc}$, $\text{Ti}_{16}\text{L}_4\text{-1}/\text{HFa(a)}$ and $\text{Ti}_{16}\text{L}_4\text{-1}/\text{HFa(b)}$ by using the FID and TCD.

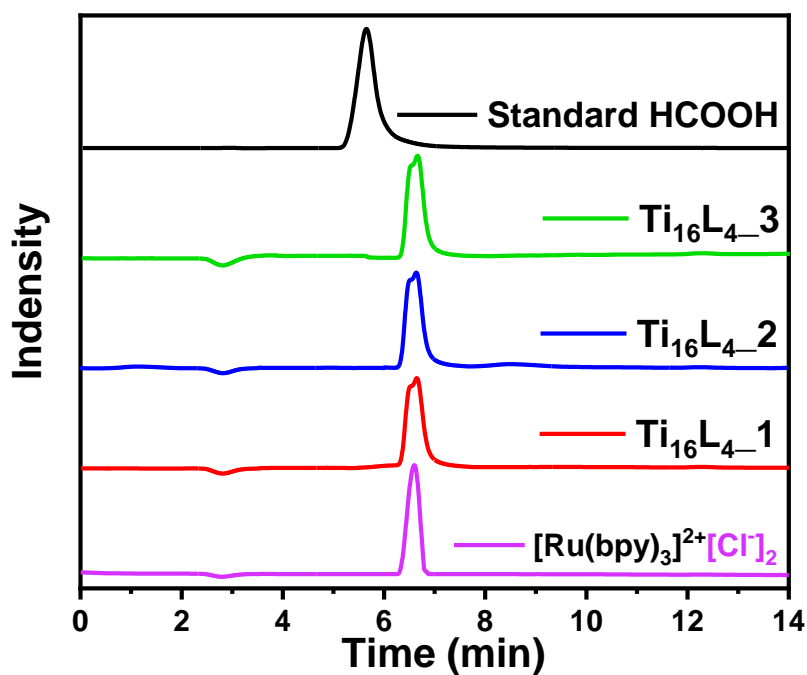


Figure S51. Analysis of the liquid reaction products generated in photocatalytic system by ion chromatography.

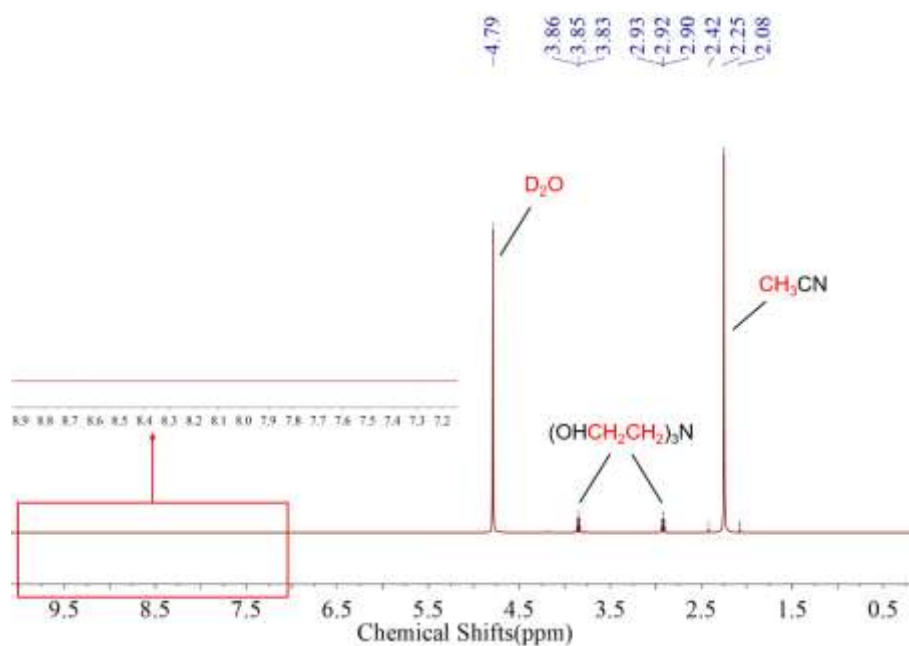


Figure S52. ¹H NMR spectrum of the liquid phase from the reaction system after visible-light irradiation.

Table S4. The photocatalysis results of the controlled experiments under different reaction conditions.

Entry	Cat.	Light	Photosensitizers	Sacrificial Agent	solvents	atmosph ere	CO/ μ mol	H ₂ / μ mol
1	Ti₁₆L4-1	Xenon lamp	[Ru(bpy) ₃]Cl ₂ ·6H ₂ O	TEOA	CH ₃ CN/H ₂ O (4:1)	CO ₂	12.02	0.07
2	Ti₁₆L4-2	Xenon lamp	[Ru(bpy) ₃]Cl ₂ ·6H ₂ O	TEOA	CH ₃ CN/H ₂ O (4:1)	CO ₂	29.99	0.44
3	Ti₁₆L4-3	Xenon lamp	[Ru(bpy) ₃]Cl ₂ ·6H ₂ O	TEOA	CH ₃ CN/H ₂ O (4:1)	CO ₂	60.57	2.34
4	×	Xenon lamp	[Ru(bpy) ₃]Cl ₂ ·6H ₂ O	TEOA	CH ₃ CN/H ₂ O (4:1)	CO ₂	0.325	0
5	Ti₁₆L4-1	Dark	[Ru(bpy) ₃]Cl ₂ ·6H ₂ O	TEOA	CH ₃ CN/H ₂ O (4:1)	CO ₂	0	0
6	Ti₁₆L4-1	Xenon lamp	[Ru(bpy) ₃]Cl ₂ ·6H ₂ O	×	CH ₃ CN/H ₂ O (4:1)	CO ₂	0.467	0.125
7	Ti₁₆L4-1	Xenon lamp	[Ru(bpy) ₃]Cl ₂ ·6H ₂ O	TEOA	CH ₃ CN/H ₂ O (4:1)	N ₂	0	0.803
8	Ti₁₆L4-1	Xenon lamp	Tris(2-phenylpyridinato)iridium	TEOA	CH ₃ CN/H ₂ O (4:1)	CO ₂	0.239	0.968
9	Ti₁₆L4-1	Xenon lamp	[Ru(bpy) ₃]Cl ₂ ·6H ₂ O	TEOA	H ₂ O	CO ₂	0.139	0.868

^a Reaction conditions: catalyst (3mg), photosensitizer (10 mg), sacrificial agent (TEOA, 5 mL), solvent (10 mL), reaction time(5 h);

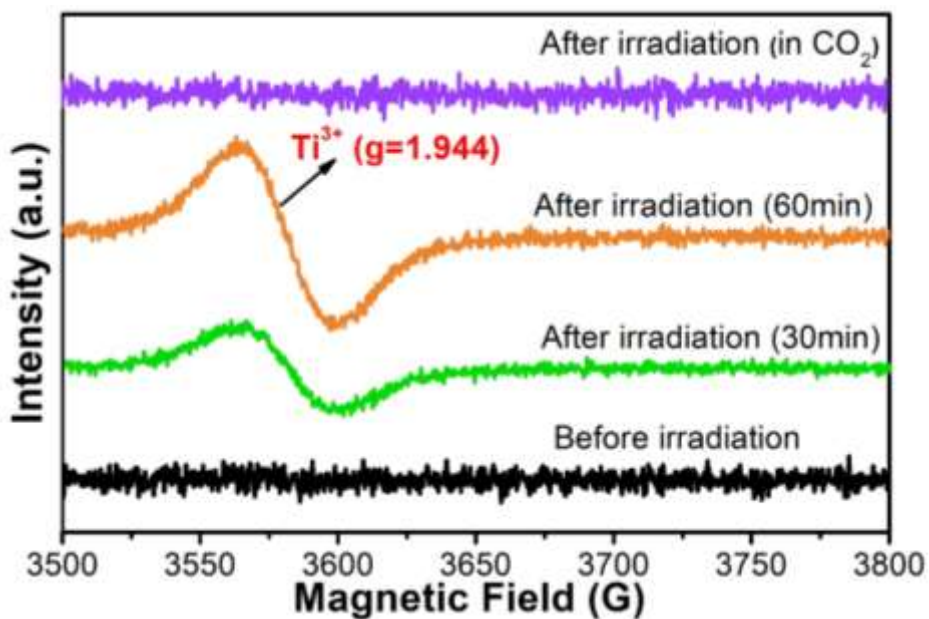


Figure S53. ESR spectrum of $\text{Ti}_{16}\text{L}_4\text{-1}$ cluster before and after light irradiation. ESR spectra were obtained on a Bruker A300 spectrophotometer at 298 K. EPR spectra were obtained using 1–20 mW microwave power and 100 kHz field modulation with the amplitude set to 1 G. The g-values for each EPR spectrum were extracted from simulations performed using EasySpin (v5.2.23).

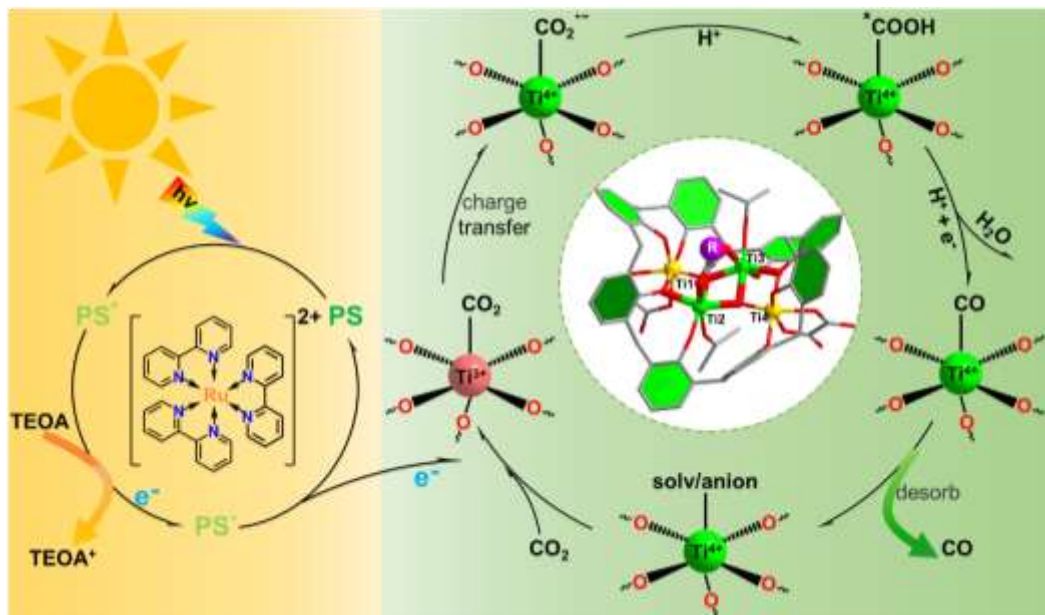


Figure S54. Reaction mechanism diagram.

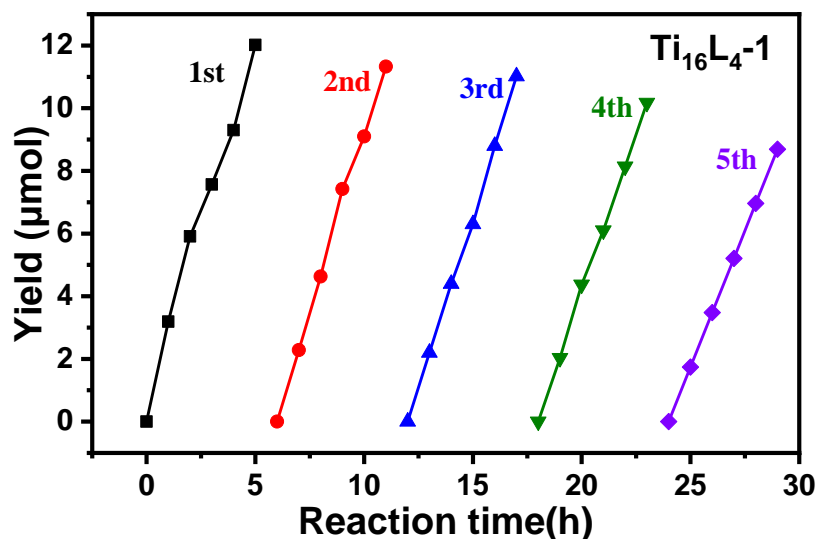


Figure S55. The photocatalysis results of the controlled experiments under different reaction conditions.

Table S5. The catalytic activity comparison of potential active sites in **Ti₁₆L₄-1/2/3**.

Entry	CO yield	TON	TON _{Ti}
Ti ₁₆ L ₄ _3	50.67 μmol	120.69	15.09
Ti ₁₆ L ₄ _2	29.99 μmol	70.96	8.87
Ti ₁₆ L ₄ _1	12.02 μmol	28.25	3.53

Turnover number (TON) = mol (CO yield) / mol (catalyst)

Turnover number (TON_{Ti}) = mol (CO yield) / mol (Ti⁴⁺ active sites)

We have demonstrated through experiments that Ti₁₆L₄ has 8 flexible coordination sites, namely active sites.

Table S6. Performance comparison of cluster-based photocatalysts for photocatalytic CO₂ reduction.

Photocatalyst	Photosensitizers	Sacrificial Agent	Reaction solvent	CO/μmol	H ₂ /μmol	Reference
Co-MOF-74	[Ru(bpy) ₃]Cl ₂ ·6H ₂ O	TEOA	Acetonitrile/H ₂ O	11.7/0.5 h	7.3/0.5 h	1
Mn-MOF-74	[Ru(bpy) ₃]Cl ₂ ·6H ₂ O	TEOA	Acetonitrile/H ₂ O	1.5/0.5 h	2.9/0.5 h	1
Zn-ZIF-8	[Ru(bpy) ₃]Cl ₂ ·6H ₂ O	TEOA	Acetonitrile/H ₂ O	2.1/0.5 h	2.4/0.5 h	1
Co ₆ -MOF	[Ru(bpy) ₃]Cl ₂ ·6H ₂ O	TEOA	Acetonitrile/H ₂ O	39.36/2 h	28.13/2 h	1
Co-ZIF-9	[Ru(bpy) ₃]Cl ₂ ·6H ₂ O	TEOA	Acetonitrile/H ₂ O	41.8/0.5 h	29.9/0.5 h	2
CuNi-L ²	[Ru(bpy) ₃]Cl ₂ ·6H ₂ O	TEOA	Acetonitrile/H ₂ O	4.6/8 h	0.32/8 h	3
TCOF-MnMo ₆	without	without	H ₂ O	7.97/24 h	—	4
RO-4	without	without	H ₂ O	0.4/4 h	—	5
Co(P ₄ Mo ₆)	[Ru(bpy) ₃]Cl ₂ ·6H ₂ O	TEOA	H ₂ O	0.32/10 h	0.012/10 h	6
Co ₁₆ -V ₄	[Ru(phen) ₃](PF ₆) ₂	TEOA	H ₂ O	3.41/10 h	—	7
Au@NENU-10	without	without	H ₂ O	1.28/5 h	0.26/5 h	8
BIF-29	[Ru(bpy) ₃]Cl ₂ ·6H ₂ O	TEOA	H ₂ O	166.7/5 h	35.0/5 h	9
Ti ₁₆ L ₄ -3	[Ru(bpy) ₃]Cl ₂ ·6H ₂ O	TEOA	Acetonitrile/H ₂ O	60.57/5 h	2.34/5 h	This work
Ti ₁₆ -C4A	without	TEOA	H ₂ O	HCOOH 136.0/12 h	—	10
PTi ₁₆	without	TEOA	H ₂ O	HCOOH 24.13/18 h	0.1/18 h	11
Ti ₆ -Fcdc	without	TIPA	H ₂ O	HCOOH 35.0/10 h	—	12
Ti ₄ -C8A	without	TEOA	H ₂ O	HCOOH 41.51/17 h	1.07/17 h	13

Reference

- Zhao, J., Wang, Q., Sun, C.Y., Zheng, T. T., Yan, L.K., Li, M. T., Shao, K. Z., Wang, X. L. & Su, Z. M. A hexanuclear cobalt metal–organic framework for efficient CO₂ reduction under visible light. *J. Mater. Chem. A*. 2017, **5**, 12498.
- Wang, S. B., Yao, W. S., Lin, J. L., Ding Z. X. & Wang, X. C. Cobalt Imidazolate Metal–Organic Frameworks Photosplit CO₂ under Mild Reaction Conditions. *Angew. Chem. Int. Ed.* 2014, **53**, 1034-1038.
- Yuan, L., Zhang, L., Li, X.-X., Liu, J., Liu, J.-J., Dong, L.-Z., Li, D.-S., Li, S.-L. & Lan, Y.-Q. Uncovering the synergistic photocatalytic behavior of bimetallic molecular catalysts. *Chinese Chem. Lett.* 2023, **34** 107146.
- Li, Q., Chang, J.-N., Wang, Z., Lu, M., Guo, C., Zhang, M., Yu, T.-Y., Chen, Y., Li, S.-L., & Lan, Y.-Q. Modulated Connection Modes of Redox Units in Molecular Junction Covalent Organic Frameworks for Artificial Photosynthetic Overall Reaction. *J. Am. Chem. Soc.*, 2022, **144**, 1861–1871.
- Li, X.-X., Zhang, L., Yuan, L., Wang, T., Dong, L.Z., Huang, K., Liu, J. & Lan, Y.-Q. Constructing crystalline redox catalyst to achieve efficient CO₂ photoreduction reaction in water vapor. *Chem. Eng. J.* 2022, **442**, 136157.
- J. Du, Y. Ma, X. Xin, H. Na, Y. Zhao, H. Tan, Z. Han, Y. Li, Z. Kang, Reduced polyoxometalates and bipyridine ruthenium complex forming a tunable photocatalytic system for high efficient CO₂ reduction, *Chem. Eng. J.* 2020, **398** 125518.
- Qiao, L., Song, M., Geng, A. & Yao, S. Polyoxometalate-based high-nuclear cobaltvanadiumoxo cluster as efficient catalyst for visible light-driven CO₂ reduction, *Chin. Chem. Lett.* 2019, **30**, 1273e1276.
- S.-M. Liu, Z. Zhang, X. Li, H. Jia, M. Ren, S. Liu, Ti-substituted keggin-type polyoxotungstate as proton and electron reservoir encaged into metaleorganic framework for carbon dioxide photoreduction, *Adv. Mater. Interfaces* 2018, **5**, 1801062.
- Zhang, H.-X., Hong, Q.-L., Li, J., Wang, F., Huang, X., Chen, S., Tu, W., Yu, D., Xu, R., Zhou, T. & Zhang, J. Isolated Square-Planar Copper Center in Boron Imidazolate Nanocages for Photocatalytic Reduction of CO₂ to CO, *Angew. Chem. Int. Ed.* 2019, **58**, 11752–11756.
- Li, N., Lin, J.-M., Li, R.-H., Shi, J.-W., Dong, L.-Z., Liu, J., He, J., & Lan, Y.-Q. Calix[4]arene-Functionalized Titanium-Oxo Compounds for Perceiving Differences in Catalytic Reactivity Between Mono- and Multimetallic Sites. *J. Am. Chem. Soc.* 2023, **145**, 16098–16108.
- Li, N., Liu, J., Liu, J.-J., Dong, L.-Z., Li, S.-L., Dong, B.-X., Kan, Y.-H. & Y.Q. Lan, Self-Assembled of a phosphate-centered polyoxo-titanium cluster: discovery of the HeteroatomKeggin family, *Angew. Chem. Int. Ed.* 2019, **58**, 17260e17264.
- Liu, J.-J., Li, N., Sun, J.-W., Liu, J., Dong, L.-Z., Yao, S.-J., Zhang, L., Xin, Z.-F., Shi, J.-W., Wang, J.-X., Li, S.-L., & Lan, Y.-Q. Ferrocene-Functionalized Polyoxo-Titanium Cluster for CO₂ Photoreduction. *ACS Catal.* 2021, **11**, 4510–4519.
- Li, N., Liu, J.-J., Sun, J.-W., Dong, B.-X., Dong, L.-Z., Yao, S.-J., Xin, Z., Li, S.-L., & Lan, Y.-Q. Calix[8]arene-constructed stable polyoxo-titanium clusters for efficient CO₂ photoreduction. *Green Chem.* 2020, **22**, 5325-5332.

Table S7 Overview of photocatalytic CO production using Ti₁₆L₄ derivatives as catalysts.

Sample	Ti ₁₆ L ₄ -1	Ti ₁₆ L ₄ -2	Ti ₁₆ L ₄ -3	Ti ₁₆ L ₄ -1/NaOH	Ti ₁₆ L ₄ -1/HFa(a)	Ti ₁₆ L ₄ -1/HFa(b)	Ti ₁₆ L ₄ -1/HAC
CO production ($\mu\text{mol g}^{-1} \text{h}^{-1}$)	798.37± 44.97	1998.10± 158.15	4046.67± 243.33	158.24 ± 85.28	911.71±115.65	636.23±19.36	773.87±43.91

Sample	Ti ₁₆ L ₄ -1/H ₂ Oa	Ti ₁₆ L ₄ -1/HGa	Ti ₁₆ L ₄ -1/HBra	Ti ₁₆ L ₄ -1/HCl _a	Ti ₁₆ L ₄ -1/HAm _a	Ti ₁₆ L ₄ -2/HTfa
CO production ($\mu\text{mol g}^{-1} \text{h}^{-1}$)	1535.04±101.19	961.19±89.20	2404.16±172.73	2632.14±210.71	1228.07±140.51	3879.07±207.31

Table S8: Crystallographic data of Ti₁₆L₄-1 after photocatalytic reaction (after five cycle).

Conditions	as-synthesized	After photocatalytic reaction
CCDC	2174429	2287594
Cryst. syst.	monoclinic	monoclinic
Space group	C2/c	C2/c
A[Å]	39.1900(19)	39.0491(14)
b[Å]	32.5046(16)	32.3507(12)

$c[\text{\AA}]$	38.1646(18)	37.9914(14)
$\beta/^\circ$	115.461(2)	115.3290(10)
$V[\text{\AA}^3]$	43894(4)	43379(3)
Goof	43894(4)	1.054
$R1/wR2(I > 2\sigma(I))$	0.0997/0.2961	0.0966/0.2770
$R1/wR2(\text{all data})$	0.1166/0.3132	0.1124/0.2955

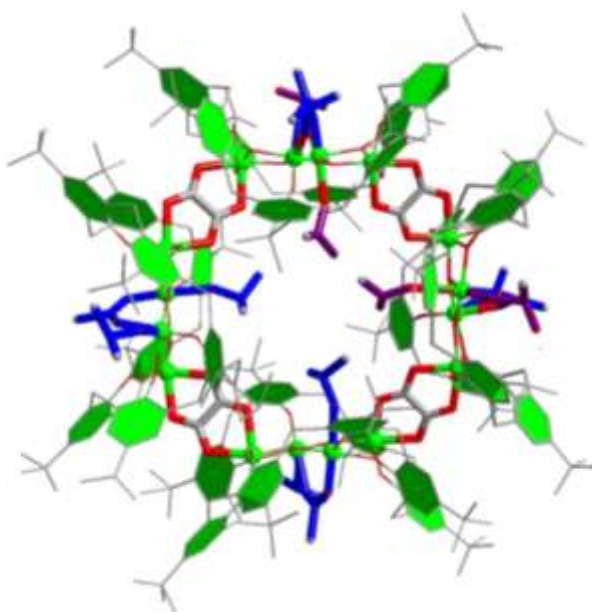


Figure S56. Crystallographic data of **Ti₁₆L₄-1** after photocatalytic reaction (after five cycle).

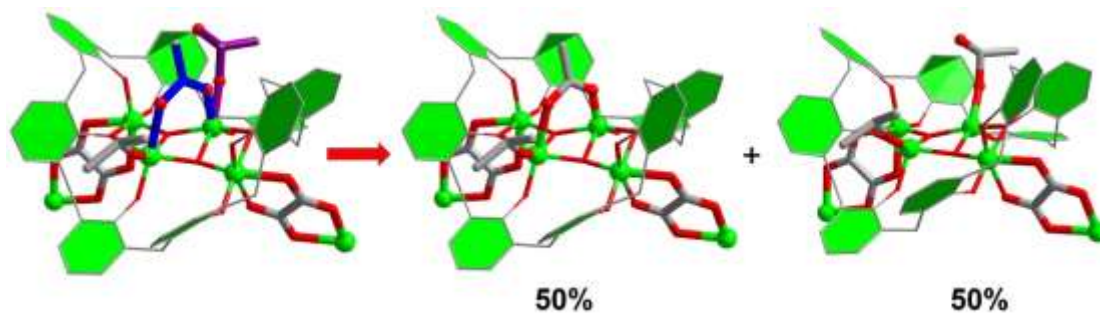


Figure S57. Crystallographic data of **Ti₁₆L₄-1** after photocatalytic reaction (after five cycle).

Discussion: After the photocatalytic reaction, the macrocyclic structure of **Ti₁₆L₄-1** remained stable, but the surface ligand changed. The ligands in the two {Ti₄-TBC[8]} subunits remain unchanged and are still occupied by one μ_2 -bridging acetate and two $^i\text{PrO}^-$ groups. However, in the other two {Ti₄-TBC[8]} subunits, the coordination mode of half of the acetate groups changed.

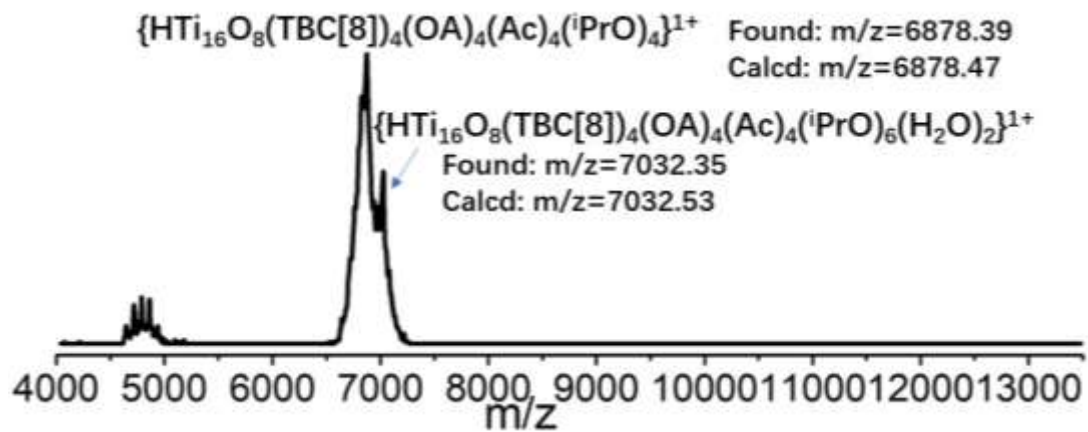


Figure S58. Positive-mode MALDI-TOF-MS spectrum of the crystalline sample of $\text{Ti}_{16}\text{L}_{4_1}$ after five catalytic cycle.

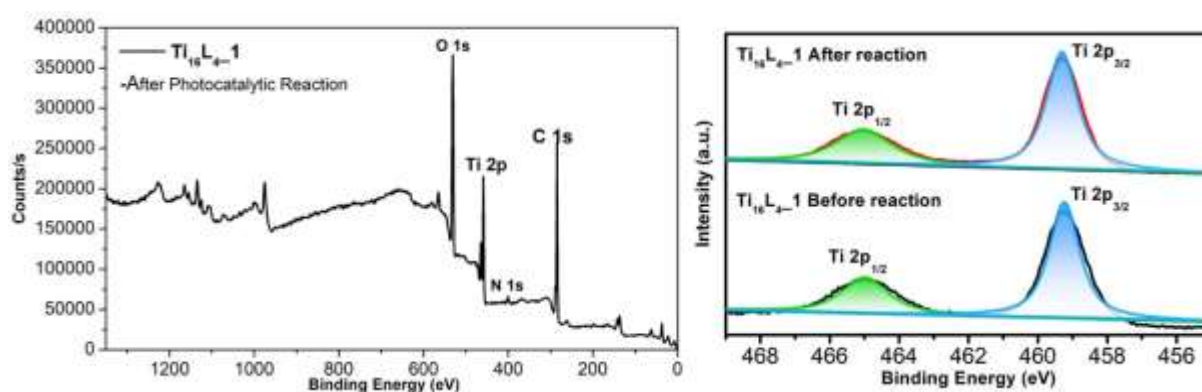


Figure S59. XPS of $\text{Ti}_{16}\text{L}_{4_1}$ after catalysis tests.

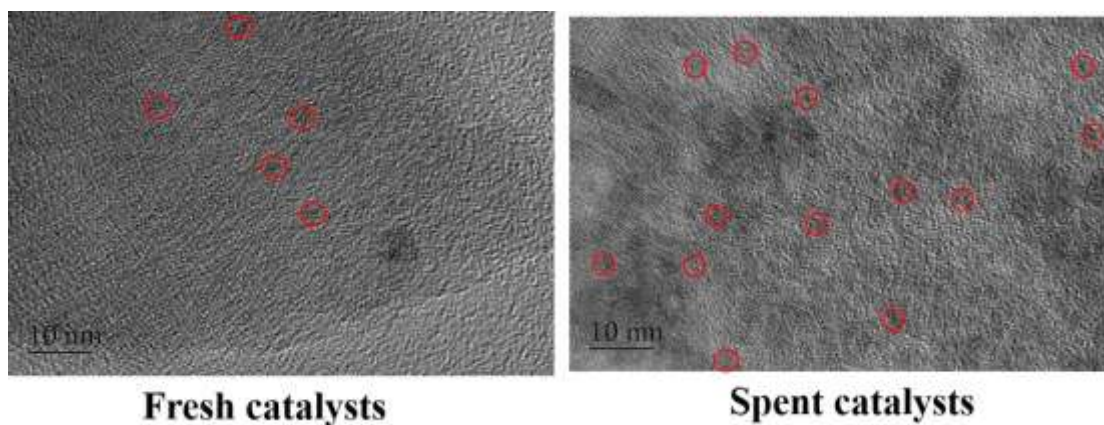


Figure S60. TEM image of $\text{Ti}_{16}\text{L}_{4_1}$ before and after reaction.